



# Role of PCIF1-mediated 5'-cap N6-methyladenosine mRNA methylation in colorectal cancer and anti-PD-1 immunotherapy

Lingling Wang<sup>1</sup>, Lujing Wu<sup>1</sup> , Zhouting Zhu<sup>1</sup>, Qiong Zhang<sup>1</sup>, Wanyu Li<sup>1</sup>, Gwendolyn Michelle Gonzalez<sup>2</sup>, Yinsheng Wang<sup>2</sup> & Tariq M Rana<sup>1,3,\*</sup> 

## Abstract

Adenosine N6-methylation (m6A) and N6,2'-O-dimethylation (m6Am) are regulatory modifications of eukaryotic mRNAs. m6Am formation is catalyzed by the methyl transferase phosphorylated CTD-interacting factor 1 (PCIF1); however, the pathophysiological functions of this RNA modification and PCIF1 in cancers are unclear. Here, we show that PCIF1 expression is upregulated in colorectal cancer (CRC) and negatively correlates with patient survival. CRISPR/Cas9-mediated depletion of PCIF1 in human CRC cells leads to loss of cell migration, invasion, and colony formation *in vitro* and loss of tumor growth in athymic mice. *Pcif1* knockout in murine CRC cells inhibits tumor growth in immunocompetent mice and enhances the effects of anti-PD-1 antibody treatment by decreasing intratumoral TGF- $\beta$  levels and increasing intratumoral IFN- $\gamma$ , TNF- $\alpha$  levels, and tumor-infiltrating natural killer cells. We further show that PCIF1 modulates CRC growth and response to anti-PD-1 in a context-dependent mechanism with PCIF1 directly targeting FOS, IFITM3, and STAT1 via m6Am modifications. PCIF1 stabilizes FOS mRNA, which in turn leads to FOS-dependent TGF- $\beta$  regulation and tumor growth. While during immunotherapy, *Pcif1*-Fos-TGF- $\beta$ , as well as *Pcif1*-Stat1/Ifitm3-IFN- $\gamma$  axes, contributes to the resistance of anti-PD-1 therapy. Collectively, our findings reveal a role of PCIF1 in promoting CRC tumorigenesis and resistance to anti-PD-1 therapy, supporting that the combination of PCIF1 inhibition with anti-PD-1 treatment is a potential therapeutic strategy to enhance CRC response to immunotherapy. Finally, we developed a lipid nanoparticles (LNPs) and chemically modified small interfering RNAs (CMsiRNAs)-based strategy to silence PCIF1 *in vivo* and found that this treatment significantly reduced tumor growth in mice. Our results therefore provide a proof-of-concept for tumor growth suppression using LNP-CMsiRNA to silence target genes in cancer.

**Keywords** anti-PD-1 treatment; colorectal carcinoma; m<sup>6</sup>Am methylation; NK cells; PCIF1

**Subject Categories** Cancer; RNA Biology

DOI 10.15252/embj.2022111673 | Received 15 May 2022 | Revised 31 October 2022 | Accepted 12 November 2022 | Published online 14 December 2022

The EMBO Journal (2023) 42: e111673

## Introduction

Despite advances in the diagnosis and treatment of colorectal cancer (CRC), it is estimated that it will account for 10% of all new cancer diagnoses and 9.4% of cancer-related deaths worldwide in 2020, placing CRC third and second, respectively, in those categories (Sung *et al.*, 2021). Bioinformatics analyses of CRC patients have identified four robust molecular subtypes of CRC: microsatellite instable, canonical oncogene alteration, metabolic activation, and transforming growth factor beta (TGF- $\beta$ )-dependent (Guinney *et al.*, 2015). Although TGF- $\beta$  signaling plays a role in several molecular CRC subtypes, the TGF- $\beta$ -dependent subtype is strongly associated with tumor angiogenesis, stromal invasion, and poor prognosis (Ikushima & Miyazono, 2010; Colak & Ten Dijke, 2017; Jung *et al.*, 2017). Physiologically, TGF- $\beta$  plays important regulatory roles in tissue homeostasis through several key cellular processes, including proliferation, differentiation, and apoptosis. However, the functions of TGF- $\beta$  in cancer depend on the context; thus, TGF- $\beta$  signaling inhibits tumorigenesis in normal epithelial cells but promotes growth and metastasis of established tumor cells (Colak & Ten Dijke, 2017). The tumor-promoting properties of TGF- $\beta$  include positive effects on intratumoral stromal cell function and angiogenesis, as well as suppression of tumor-infiltrating effector cells such as T cells and natural killer (NK) cells.

Immune checkpoint blockade (ICB) has revolutionized our approach to cancer immunotherapy. However, while antibodies targeting inhibitory receptor–ligand interactions between T cells and tumor cells, such as those mediated by programmed cell death receptor 1 (PD-1), its ligand programmed cell death ligand 1 (PD-L1), and cytotoxic T lymphocyte-associated protein 4 (CTLA-4) can elicit durable remission in some cancers, and they are ineffective against other tumor types, such as CRC (Kim *et al.*, 2014).

1 Division of Genetics, Department of Pediatrics, Program in Immunology, Bioinformatics and Systems Biology Program, University of California San Diego, La Jolla, CA, USA

2 Environmental Toxicology Graduate Program and Department of Chemistry, University of California, Riverside, CA, USA

3 San Diego Center for Precision Immunotherapy, University of California San Diego, La Jolla, CA, USA

\*Corresponding author. Tel: +1 858 246 1100; E-mail: trana@ucsd.edu

Furthermore, not all patients with ICB-responsive tumors have good outcomes to targeted therapy, and identification of tumor and host factors that determine the outcomes of ICB is therefore an active area of research. For example, exclusion of certain immune cell subsets and elevated TGF- $\beta$  signaling in the tumor microenvironment (TME) are recognized as determinants of poor responses to anti-PD-1/PD-L1 therapy in some tumors, including CRC (Calon *et al*, 2015; Ganesh & Massague, 2018), which has raised the possibility that suppression of TGF- $\beta$  signaling could be used to amplify tumor responses to anti-PD-1/PD-L1 therapy.

Posttranscriptional RNA modification is emerging as an important epigenetic regulatory circuit in multiple pathophysiological contexts.  $N^6$ -methyladenosine ( $m^6A$ ) is the most abundant mRNA modification in mammals and is generally located at the 5'- and 3'-untranslated regions (UTRs) and stop codons (Dominissini *et al*, 2012; Meyer *et al*, 2012; Schwartz *et al*, 2014). The abundance of  $m^6A$  in cellular RNA metabolism is regulated by the activity of the methyltransferases METTL3/14 (Liu *et al*, 2014) ("writers"), the YTH family of  $m^6A$ -binding proteins (Wang *et al*, 2014, 2015; Xiao *et al*, 2016; Li *et al*, 2017) ("readers"), and demethylases such as ALKBH5 (Zheng *et al*, 2013) ("erasers"). Recent studies have identified roles for  $m^6A$  in various diseases (Hess *et al*, 2013; Satterlee *et al*, 2014) including cancer (Barbieri *et al*, 2017; Vu *et al*, 2017; Su *et al*, 2018; Han *et al*, 2019; Paris *et al*, 2019; Yang *et al*, 2019), and in the response of cancer to immunotherapy. For example, knock-down of YTHDF1 and the demethylase FTO were shown to enhance the response of melanoma tumors to anti-PD-1 therapy (Han *et al*, 2019; Yang *et al*, 2019). In addition, we recently showed that deletion of ALKBH5 sensitized melanoma tumors to immunotherapy and prolonged mouse survival through a mechanism involving modulation of lactate levels in the TME, which, in turn, regulated accumulation of immunosuppressive T regulatory lymphocytes (Tregs) and myeloid-derived suppressor cell (MDSCs) in the TME (Li *et al*, 2020). We also found that inhibition of  $m^6A$  modification by depletion of Mettl3 and Mettl14 enhanced the response of pMMR-MSI-L CRC and melanoma to anti-PD-1 treatment (Wang *et al*, 2020). Consequently, inhibitors targeting enzymes regulating  $m^6A$  pathways are being developed as potential new therapeutics to treat multiple cancers (Li *et al*, 2020; Huff *et al*, 2021, 2022; Yankova *et al*, 2021).

Another abundant RNA modification located near the mRNA cap structure is the dimethylated  $N^6,2'$ - $O$ -dimethyladenosine ( $m^6Am$ ) (Wei *et al*, 1975; Keith *et al*, 1978).  $m^6Am$  is located at the first transcribed nucleotide in ~ 30% of cellular mRNAs and thus can have a major influence on the transcriptome (Wei *et al*, 1975). Recent studies identified the methylase phosphorylated CTD-interacting factor 1 (PCIF1) as the enzyme that catalyzes  $m^6Am$  methylation of 2'- $O$ -methylated adenosine at the 5'-end of mRNAs (Akichika *et al*, 2019; Boulias *et al*, 2019; Sendinc *et al*, 2019; Sun *et al*, 2019). However, the pathophysiological roles of  $m^6Am$  and PCIF1 are unclear. Two recent studies revealed the function of PCIF1 in modulating HIV and VSV pathogenesis and immune responses (Tartell *et al*, 2021; Zhang *et al*, 2021). During HIV infection, viral protein Vpr degrades PCIF1 and reprograms human T cells  $m^6Am$  methylome. In VSV, PCIF1 modifies viral mRNA cap structure and attenuates the antiviral effects of interferon-beta (Tartell *et al*, 2021). In the present study, we set out to determine the role of  $m^6Am$  modification in CRC and its response to anti-PD-1 immunotherapy. We found that PCIF1 is

highly expressed in human CRC tumors and correlates with poor patient prognosis and that PCIF1-mediated  $m^6Am$  modification of the classical oncogene FOS promotes CRC malignant behaviors and suppresses the response to anti-PD-1 immunotherapy in mouse tumor models. Thus, our results identify a novel role for  $m^6Am$  in tumor biology and also raise the possibility that  $m^6Am$ -regulating pathways could serve as therapeutic targets for cancer both directly and by sensitizing refractory tumors to ICB therapy.

## Results

### PCIF1 is overexpressed in CRC and correlates with poor survival

To determine whether  $m^6Am$ , like  $m^6A$ , may play a role in cancer development and response to therapy, we first examined the expression level of PCIF1 in multiple cancers by analyzing RNA-seq data sets using TIMER2.0 database. This analysis showed that PCIF1 was significantly elevated in several tumors, including CRC ( $n = 457$ ), compared with adjacent normal tissues ( $n = 41$ ; Fig EV1A). To verify these results, we performed immunohistochemical (IHC) staining of PCIF1 protein in 27 matched pairs of CRC and normal tissues. We found that PCIF1 was expressed at much higher levels in tumor cells compared with normal colon cells and was mainly localized to the nucleus (Fig 1A). Moreover, of those 27 patients, 19 patients whose tumors were classified as having low PCIF1 expression survived significantly longer than did the eight patients with high PCIF1 levels (Fig 1B). However, PCIF1 staining intensity did not correlate with stage, pathology grade, gender, or age in 70 patients with CRC (Fig EV1B). These results therefore demonstrate that PCIF1 is overexpressed in CRC and that high expression correlates with poor survival.

We further investigated the PCIF1 expression level in multiple established CRC cell lines and a normal human colon cell line. Western blot and qRT-PCR analysis revealed that PCIF1 is expressed at higher levels in CRC cell lines compared with normal colon cells at both the protein and mRNA levels (Fig 1C and D). Moreover, PCIF1 was localized predominantly in the nucleus of HCT116 and HT29 CRC cells, as measured by immunofluorescence staining (Fig 1E) and subcellular fractionation followed by immunoblotting (Fig 1F). These results confirm that the human CRC cell lines effectively phenocopy human CRC tissues in both the elevated expression and nuclear localization of PCIF1.

### PCIF1 depletion suppresses the malignant behavior of CRC cells *in vitro* and *in vivo*

Because the functional role of PCIF1 in CRC is not known, we examined the growth and malignant behaviors of cell lines subjected to PCIF1 knockout by CRISPR/Cas9 editing with *PCIF1*-specific single-guide RNA (sgRNA). Western blot analysis of HCT116 and HT29 cells showed that PCIF1 protein was effectively reduced by infection with *PCIF1* sgRNA compared with control sgRNA (Fig 2A). Notably, assays of cell proliferation (Fig EV1C and D), invasion (Fig 2B), fibronectin adhesion (Fig 2C), colony formation (Fig 2D), and migration (Fig 2E) revealed that PCIF1 depletion significantly reduced all of these malignancy-associated behaviors compared with the control cells. To confirm that the effect of PCIF1 depletion

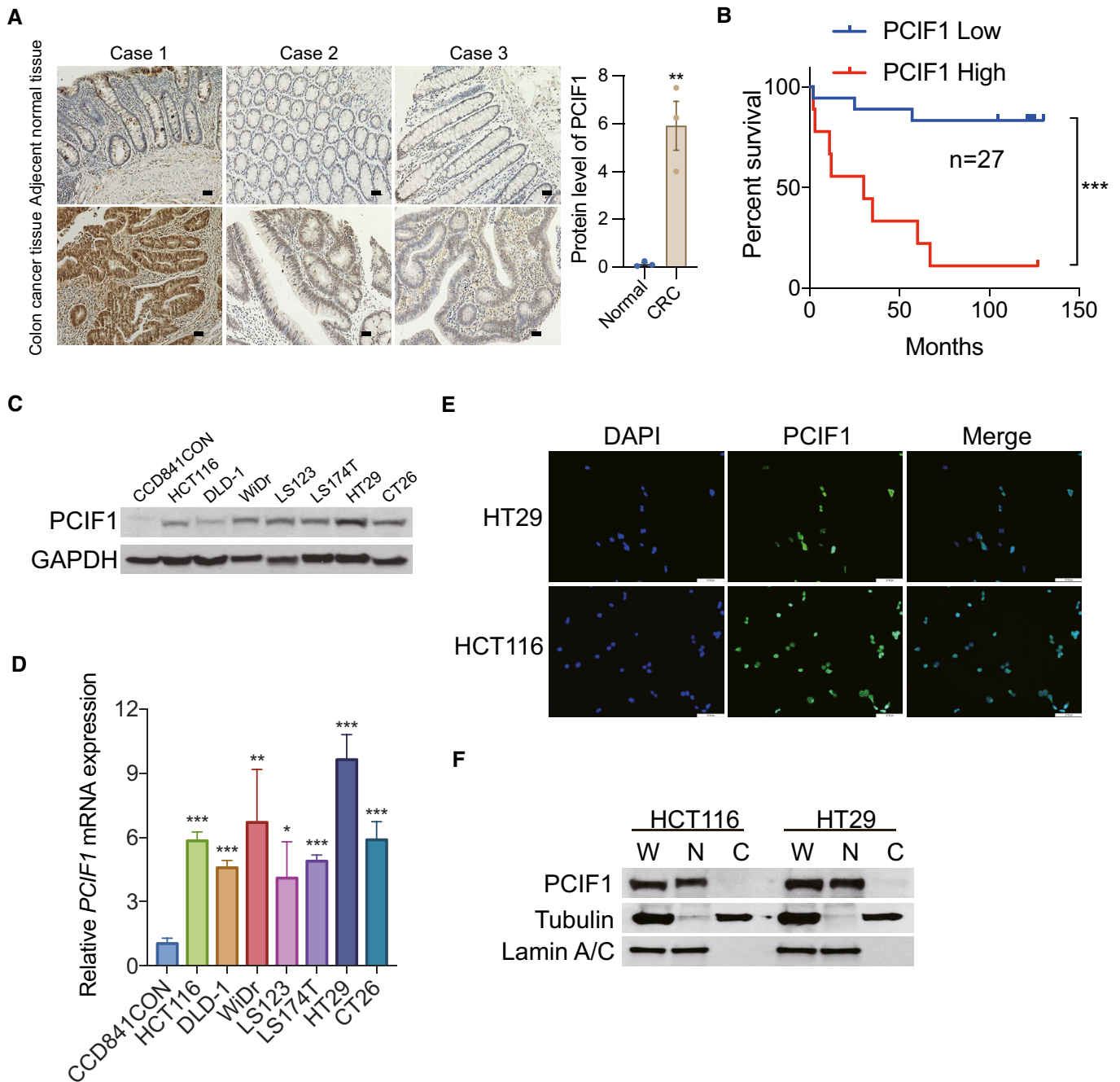


**Figure 1. PCIF1 is upregulated in CRC.**

- A Representative images of IHC staining of PCIF1 in three CRC tissues and adjacent noncancerous tissues. Scale bar, 50  $\mu$ m (left). Analysis of the PCIF1 protein expression in normal and CRC tissues. Each dot represents one sample (right). Data are the mean  $\pm$  SEM. \*\* $P$  < 0.01, by Student's  $t$ -test.
- B Kaplan–Meier plots of overall survival of 27 CRC patients with low tumor PCIF1 expression (0–4.5 staining score,  $n$  = 18) or high tumor PCIF1 expression (4.6–9.0 staining score,  $n$  = 9). Data are the mean  $\pm$  SEM. \*\*\* $P$  < 0.001 by Student's  $t$ -test.
- C Western blot analysis of PCIF1 in normal colon cells (CCD841CON) and various CRC cell lines. GAPDH served as a loading control.
- D qRT-PCR analysis of *PCIF1* mRNA in the indicated cell lines. Levels were normalized to GAPDH expression. Data are the mean  $\pm$  SD of  $n$  = 3 biological replicates. \* $P$  < 0.05, \*\* $P$  < 0.01, \*\*\* $P$  < 0.001 by Student's  $t$ -test.
- E Representative immunofluorescence images of HT29 and HCT116 cells stained for endogenous PCIF1 protein (green). Nuclei were stained with DAPI (blue). Scale bar, 30  $\mu$ m.
- F Western blot analysis of PCIF1 in whole extract (W), cytosolic (C), and nuclear (N) fractions of HCT116 and HT29 cells. Tubulin and lamin A/C served as cytosolic and nuclear markers, respectively.

Source data are available online for this figure.

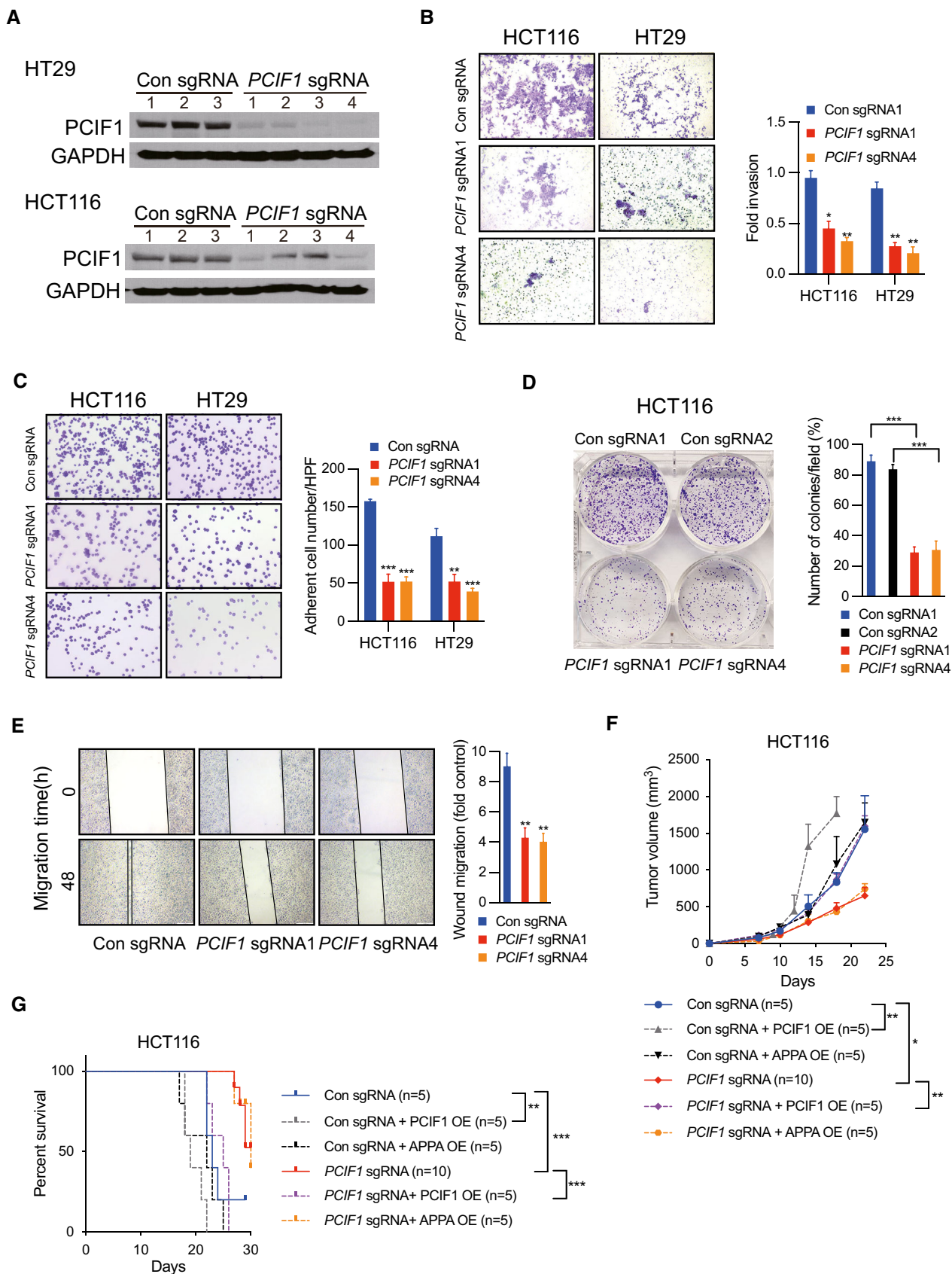


Figure 2.

**Figure 2. PCIF1 depletion reduces CRC tumorigenesis.**

- A Western blot analysis of PCIF1 in HT29 and HCT116 cells depleted of PCIF1 using four different sgRNAs. GAPDH served as a loading control.
- B–E Matrigel invasion assay (B), fibronectin adhesion assay (C), colony formation assay (D), and wound healing migration assay (E) of the indicated control and PCIF1-depleted CRC cell lines. Representative images and quantification of cells are shown at the left and right, respectively, of each panel. Data are the mean  $\pm$  SD of  $n = 3$  replicates/condition. \* $P < 0.05$ , \*\* $P < 0.01$ , \*\*\* $P < 0.001$  by Student's *t*-test.
- F Growth of the indicated HCT116 tumors after subcutaneous injection into athymic nude mice. Tumor volume was recorded on the indicated days. Data are the mean  $\pm$  SEM of the number of mice/group indicated on each panel.  $n$ , the numbers of mice. \* $P < 0.05$ , \*\* $P < 0.01$  by Student's *t*-test.
- G Survival analysis of mice injected bearing the indicated HCT116 tumors. Data are the mean  $\pm$  SEM of the number of mice/group indicated on each panel.  $n$ , the numbers of mice. \*\* $P < 0.01$ , \*\*\* $P < 0.001$  by Student's *t*-test.

Source data are available online for this figure.

on CRC growth was not restricted to the *in vitro* conditions, PCIF1-depleted HCT116 tumor cells were injected subcutaneously into athymic nude mice. Indeed, PCIF1-depleted tumors grew significantly more slowly than control tumors (Fig 2F) and mice bearing the PCIF1-depleted tumors survived significantly longer than control tumor-bearing mice (Fig 2G). Furthermore, IHC staining of the proliferation marker Ki-67 in sections of tumors confirmed significantly reduced Ki-67 expression levels in PCIF1-depleted tumors compared with control tumors (Fig EV1E). Collectively, these results indicate that PCIF1 plays a pivotal role in promoting the growth of CRC. To further determine whether the methyltransferase activity of PCIF1 is required for enhancing CRC tumor growth, we performed rescue experiments by overexpressing either sgRNA resistant (sgRNA R) wild-type PCIF1 or catalytically inactive PCIF1 (APPA) mutant (Zhang *et al*, 2021) in the control sgRNA and PCIF1 knockout cells (Fig EV1F) and analyzed the tumor growth. In the control sgRNA group, overexpression of wild-type PCIF1, but not APPA mutant, enhanced tumor growth and shortened the mice survival (Fig 2F and G). Accordingly, in PCIF1-deficient group, only the overexpression of wild-type PCIF1, and not the APPA mutant, rescued the tumor suppression caused by PCIF1 depletion and shortened the animal survival (Fig 2F and G). These results demonstrate that catalytically active PCIF1 contributes to promoting tumor growth.

**Identification of potential target genes of PCIF1 in CRC**

To understand the molecular mechanisms by which PCIF1 promotes the growth and malignant behaviors of CRC, we first determined whether PCIF1 mediates deposition of  $m^6A$  in CRC cell RNA. Using an LC-MS/MS protocol (Li *et al*, 2020; Huff *et al*, 2021), we examined the ratios of  $m^6A$  and  $m^6Am$  to unmethylated adenosine ( $m^6A/A$  and  $m^6Am/A$ , respectively) in total mRNA from control and PCIF1-depleted HCT116 cells. We found that PCIF1 silencing significantly reduced the ratio of  $m^6Am/A$ , but not  $m^6A/A$ , compared with control cells, which is consistent with previous findings (Fig 3A; Sendinc *et al*, 2019). Next, we performed RNA sequencing (RNA-seq) and  $m^6Am$ -exo-Seq (Sendinc *et al*, 2019) to identify genome-wide changes in total mRNA and  $m^6Am$ -modified mRNA, respectively. From the  $m^6Am$ -exo-seq analysis, we found a clear enrichment of 5' ends around transcription start sites (TSS) in control mRNA rather than PCIF1-depleted mRNA by metagene plots of  $m^6Am$  enrichment analysis, indicating that these transcripts are likely  $m^6Am$  modified (Fig 3B). The RNA-seq analysis identified 464 genes that were significantly downregulated in PCIF1-depleted cells compared with control cells, and the  $m^6Am$ -exo-seq data identified 3,585 significantly decreased  $m^6Am$  peaks in PCIF1 depleted

compared with control cells. By comparing overlap between the two gene sets, we identified a total of 76 candidate genes whose expression was regulated by PCIF1-mediated  $m^6Am$  modification (Figs 3C and EV2A; Dataset EV1–EV3). Gene Ontology analysis of the function of these 76 genes revealed enrichment in pathways relevant to “regulation of epithelial cell proliferation,” “cell-cell signaling by WNT,” “regulation of cell adhesion,” and other pathways relevant to tumor growth (Fig 3D). Of particular interest, the 76 PCIF1-regulated genes were particularly highly enriched in the “response to transforming growth factor beta (TGF- $\beta$ )” pathway.

Because mutations in TGF- $\beta$  receptors and aberrant TGF- $\beta$  signaling are strongly associated with certain CRC subtypes (Xu & Pasche, 2007), we examined the involvement of PCIF1 in regulation of the TGF- $\beta$  pathway in more detail. We first performed qRT-PCR analysis of all of the genes included in the TGF- $\beta$  pathway in PCIF1-depleted and control CRC cells. This analysis confirmed the differential regulation of TGF- $\beta$ -associated genes by PCIF1 and identified the proto-oncogene *FOS* as the most significantly downregulated gene in PCIF1-depleted HCT116 and HT29 cells (Fig EV2B and C). In agreement with the qRT-PCR results, western blot analysis of CRC cells (Fig 3E) and IHC staining of HCT116 tumors from Fig 2F (Fig EV2D) confirmed that *FOS* protein expression was reduced by PCIF1 depletion in CRC. Analysis of the  $m^6Am$ -exo-seq data, which showed  $m^6Am$  on 5' ends immediate to TSS had a clear decreased peak in PCIF1-depleted cells, indicating *FOS* is a  $m^6Am$ -modified gene (Fig 3F). We further validated this result by  $m^6Am$ -exo-qPCR showing significant decrease in *FOS* mRNA levels in PCIF1-deficient cells, which is consistent with sequencing results (Fig 3G). These findings suggest that *FOS* expression is regulated by PCIF1-mediated  $m^6Am$  modification. One of the functions of 5'-cap-located  $m^6Am$  is to control mRNA stability (Boulias *et al*, 2019); therefore, we analyzed the half-life of *FOS* mRNA upon PCIF1 knockout in CRC cells. Control or PCIF1-depleted HCT116 and HT29 cells were incubated with actinomycin D to inhibit new RNA synthesis, and *FOS* mRNA levels were quantified by qRT-PCR at various times thereafter. The results showed that *FOS* mRNA was significantly less stable in PCIF1-depleted cells than in control cells (Fig 3H). Collectively, these results demonstrate that PCIF1 controls *FOS* mRNA stability in CRC cells via  $m^6Am$  deposition.

Next, we determined whether *FOS* mediates the effects of PCIF1 on CRC cell function by examining whether restoration of *FOS* expression can overcome the functional deficits of PCIF1 depletion. Control and PCIF1-depleted HCT116 and HT29 cells were transfected with a *FOS* overexpression vector, and restoration of *FOS* protein expression was confirmed by western blot analysis (Fig EV2E). We then examined the effects of *FOS* overexpression on

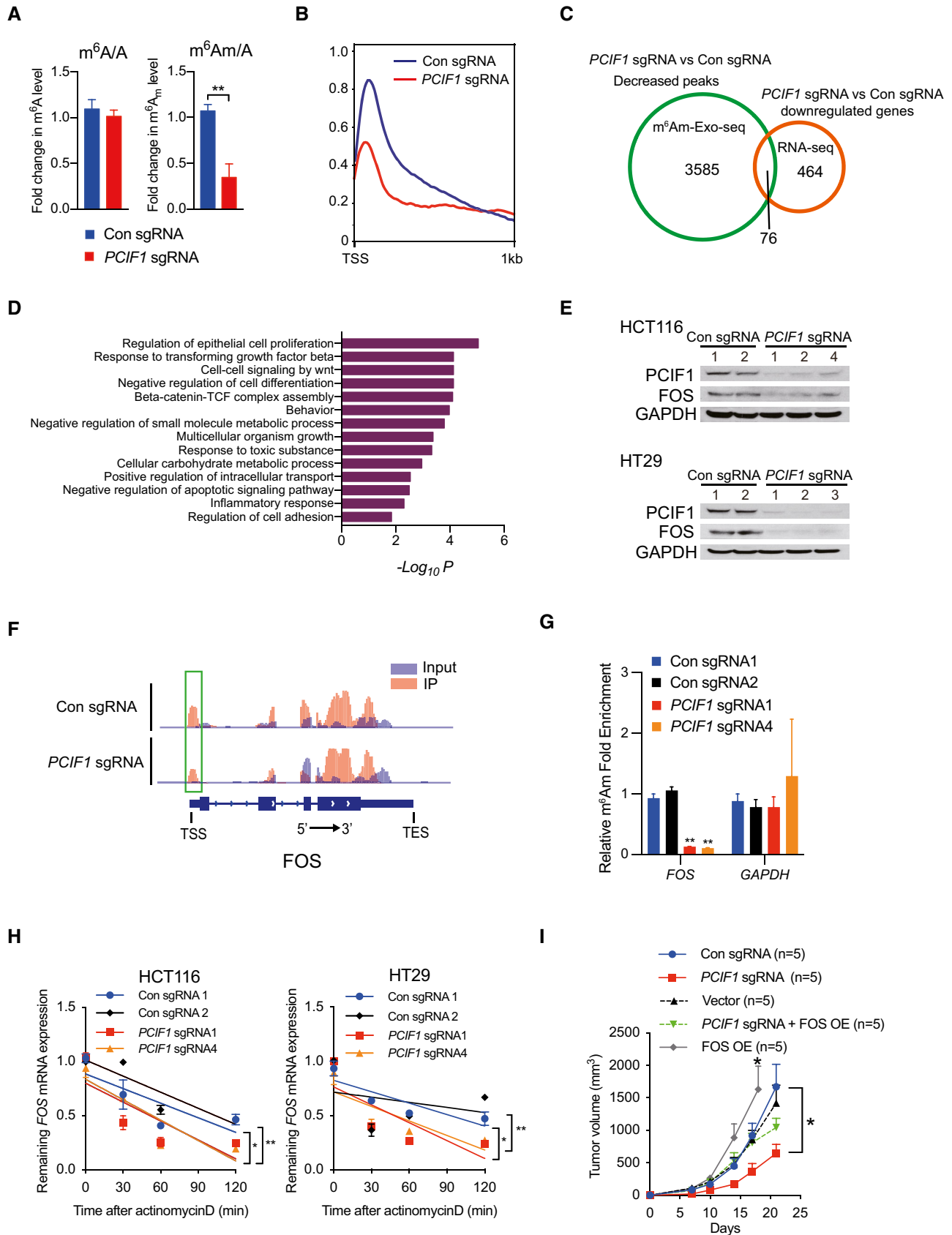


Figure 3.

**Figure 3. PCIF1 target genes identified by RNA-seq and m<sup>6</sup>Am-exo-seq.**

- A LC-MS/MS quantification of m<sup>6</sup>Am or m<sup>6</sup>A levels in mRNA from control and PCIF1-depleted HCT116 cells. Data are presented as the enrichment of methylated vs unmethylated mRNA. Data are the mean ± SD of *n* = 3 biological replicates. \*\**P* < 0.01 by Student's *t*-test.
- B Metagene plots analysis of m<sup>6</sup>Am enrichment around the transcription start site (TSS) of all expressed genes in control and PCIF1-depleted HCT116 cells.
- C Venn diagram of PCIF1 peaks number, downstream genes, and identified genes from m<sup>6</sup>Am-exo-seq and RNA-seq.
- D Meta-enrichment analysis summary for the 76 genes identified as PCIF1 targets in HCT116 cells.
- E Western blot analysis of FOS and PCIF1 in control and PCIF1-depleted HCT116 and HT29 cells. GAPDH served as a loading control.
- F Genome browser views of FOS with m<sup>6</sup>Am sites. Read coverage of input sample and IP sample are shown in blue and red, respectively, and green rectangle indicates the m<sup>6</sup>Am peaks located near the TSS.
- G m<sup>6</sup>Am-exo-qPCR analysis of m<sup>6</sup>Am enrichment in *FOS* mRNAs from the indicated HCT116 cells. GAPDH served as a negative control. Data are the mean ± SD of *n* = 3 biological replicates. \*\**P* < 0.01 by Student's *t*-test.
- H qRT-PCR analysis of *FOS* mRNA stability in control and PCIF1-depleted HCT116 and HT29 cells treated with actinomycin D for the indicated times. Data are the mean ± SD of *n* = 3 biological replicates. \**P* < 0.05, \*\**P* < 0.01 by Student's *t*-test.
- I Growth of tumors after subcutaneous injection of the indicated HCT116 cells into athymic nude mice. Tumor volumes were recorded on the indicated days. Data are the mean ± SEM of *n* = 5. \**P* < 0.05 by Student's *t*-test.

Source data are available online for this figure.

CRC cell growth *in vitro* and *in vivo*. Notably, overexpression of FOS essentially overcomes the inhibitory effects of PCIF1 depletion on HCT116 and HT29 cell proliferation *in vitro* (Fig EV2F) and tumor growth *in vivo* (Fig 3I). Furthermore, FOS overexpression alone promotes tumor growth compared with control cells (Fig 3I). These data confirm that FOS plays a role in mediating the CRC growth-promoting effects of PCIF1.

**FOS suppression inhibits CRC tumorigenesis**

FOS, a proto-oncogene, is required in malignant progress of multiple cancer types including head and neck squamous cell carcinoma (Muhammad *et al*, 2017) and skin cancer (Saez *et al*, 1995). However, little is known about the role of FOS in CRC, thus we initially explored the expression of FOS in a normal human colon cell line and numerous established human CRC cell lines and found that FOS is expressed at higher levels in CRC cell lines compared to normal colon cells at both the protein and mRNA levels determined by Western blot and qRT-PCR analyses, respectively (Fig EV3A and B). Thereafter, FOS-depleted HCT116 and HT29 cells via CRISPR/Cas9 editing was generated to investigate its function. Western blot analysis confirmed the near-complete loss of FOS protein in cells expressing *FOS*-targeted sgRNAs compared with control sgRNA (Fig 4A). Moreover, cell proliferation (Fig 4B), migration (Fig 4C), and colony formation (Fig 4D) were all markedly reduced in FOS-depleted CRC cells compared with control cells. Consistent with these *in vitro* analyses, tumors formed by FOS-depleted HCT116 cells grew significantly more slowly than control tumors (Fig 4E), and accordingly, mice bearing FOS-depleted tumors survived significantly longer than the control mice (Fig 4F). Taken together, these data indicate that FOS promotes CRC malignant behavior, consistent with a role in mediating the effects of PCIF1. Finally, we asked whether FOS expression was dysregulated similarly to PCIF1 in CRC tumor tissues. Indeed, IHC staining of tumors from 29 patients with CRC identified a significant positive correlation between PCIF1 and FOS protein levels (Fig 4G). Collectively, these data support a role for FOS in PCIF1-mediated regulation of CRC growth.

FOS is a primary member of the AP-1 family of transcription factors, is known to regulate transcription of TGF-β (Pandey *et al*, 2012; Zhou *et al*, 2020), and TGFβ has a well-characterized role in promoting CRC (Xu & Pasche, 2007). Given the known role of FOS in TGF-β transcription, and the link between TGF-β and CRC,

we next asked whether FOS regulates TGF-β expression in CRC, and if so, whether that occurs in a PCIF1-dependent or -independent manners. To this end, we first examined expression of the three TGF-β isoforms (TGFβ1-3) in FOS-deficient HCT116 cells and tumors from Fig 4E by qRT-PCR and immunoblot analysis, respectively. Compared with control, we found that all three isoforms were significantly reduced in FOS-depleted cells and tumors (Fig EV3C and D), indicating that FOS regulates TGF-β transcription in CRC. Notably, similar reductions in TGF-β mRNA and protein levels were also observed in PCIF1-depleted CRC cells (Fig EV3E and F), but the effects were reversed by concomitant overexpression of FOS (Fig EV3F). Thus, PCIF1 regulates TGF-β expression in CRC through FOS.

**PCIF1 sensitizes CRC to anti-PD-1 therapy**

The sensitivity of tumors to anti-PD-1 therapy appears to be influenced by a number of factors, including the composition of immune cells and cytokines within the TME (Li *et al*, 2020; Wang *et al*, 2020). Therefore, we next asked whether PCIF1 and/or FOS suppression influence anti-PD-1 effects on CRC *in vivo*, and if so, whether the effects are mediated by alteration of the TME. We first performed CRISPR/Cas9-mediated deletion of *Pcif1* in the murine CRC cell lines CT26 and MC38 and examined tumor growth in syngeneic immunocompetent mice. Efficient depletion of *Pcif1* protein in the two cell lines was confirmed by western blot analysis (Fig EV4A and B). Control and *Pcif1*-depleted CT26 and MC38 cells were injected subcutaneously into BALB/c or C57BL/6J mice, respectively, and groups of mice were then either untreated or treated with 200 μg anti-PD-1 antibody as described in methods. Intriguingly, *Pcif1* depletion alone and anti-PD-1 treatment alone both significantly inhibited the growth of CRC tumors; however, an additive effect of both treatments was observed such that tumor growth was virtually abolished in anti-PD-1 antibody-treated animals bearing *Pcif1*-depleted tumors (Fig 5A and B). These results indicate that *Pcif1* depletion further sensitizes CRC tumors to the growth inhibitory effects of anti-PD-1 therapy in immunocompetent mice.

To identify the potential mechanisms by which *Pcif1* depletion enhanced the effects of anti-PD-1 on CRC tumor growth, we performed flow cytometry to analyze the composition of tumor-infiltrating cells in CT26 tumors after subcutaneous injection into

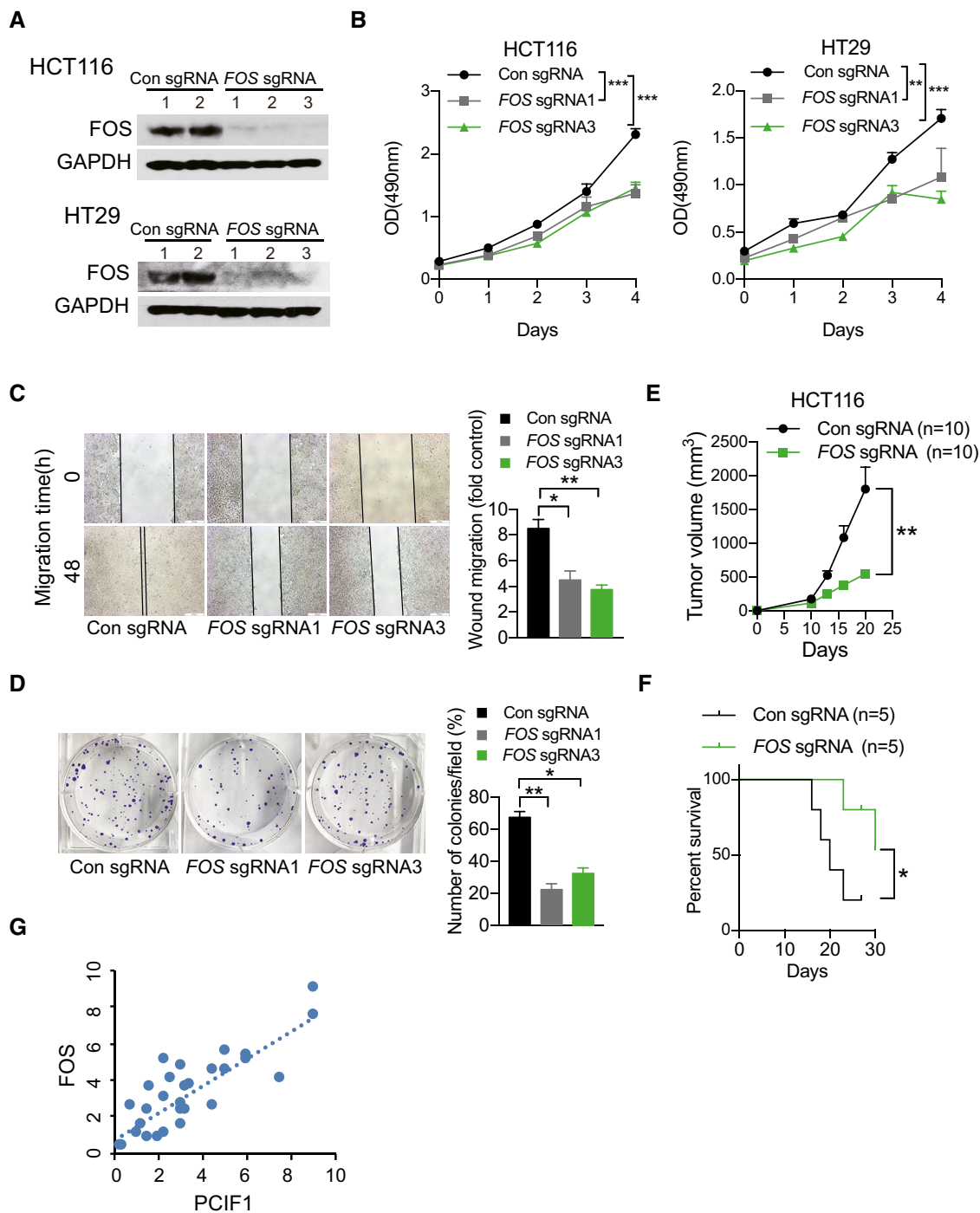


**Figure 4. Functional role of FOS in CRC.**

- A Western blot analysis of FOS in control and FOS-depleted HCT116 and HT29 cells. GAPDH served as a loading control.
- B–D MTS cell proliferation assay (B), wound healing migration assay (C), and colony formation assay (D) of control and FOS-depleted HCT116 cells. Representative images and quantification of colonies are shown to the left and right, respectively. Data are the mean  $\pm$  SD of  $n = 3$  biological replicates. \* $P < 0.05$ , \*\* $P < 0.01$ , \*\*\* $P < 0.001$  by Student's  $t$ -test.
- E Growth of control and FOS-depleted HCT116 tumors after subcutaneous injection into athymic nude mice. Tumor volume was recorded on the indicated days. Data are the mean  $\pm$  SEM of  $n = 10$  mice/group. \*\* $P < 0.01$  by Student's  $t$ -test.
- F Survival analysis of mice bearing control and FOS-depleted HCT116 tumors. Data are the mean  $\pm$  SEM of  $n = 5$  mice/group. \* $P < 0.05$  by Student's  $t$ -test.
- G Positive correlation between FOS and PCIF1 protein levels in tumors from 29 patients with CRC ( $R^2 = 0.6902$ ,  $P < 0.001$ ).

Source data are available online for this figure.



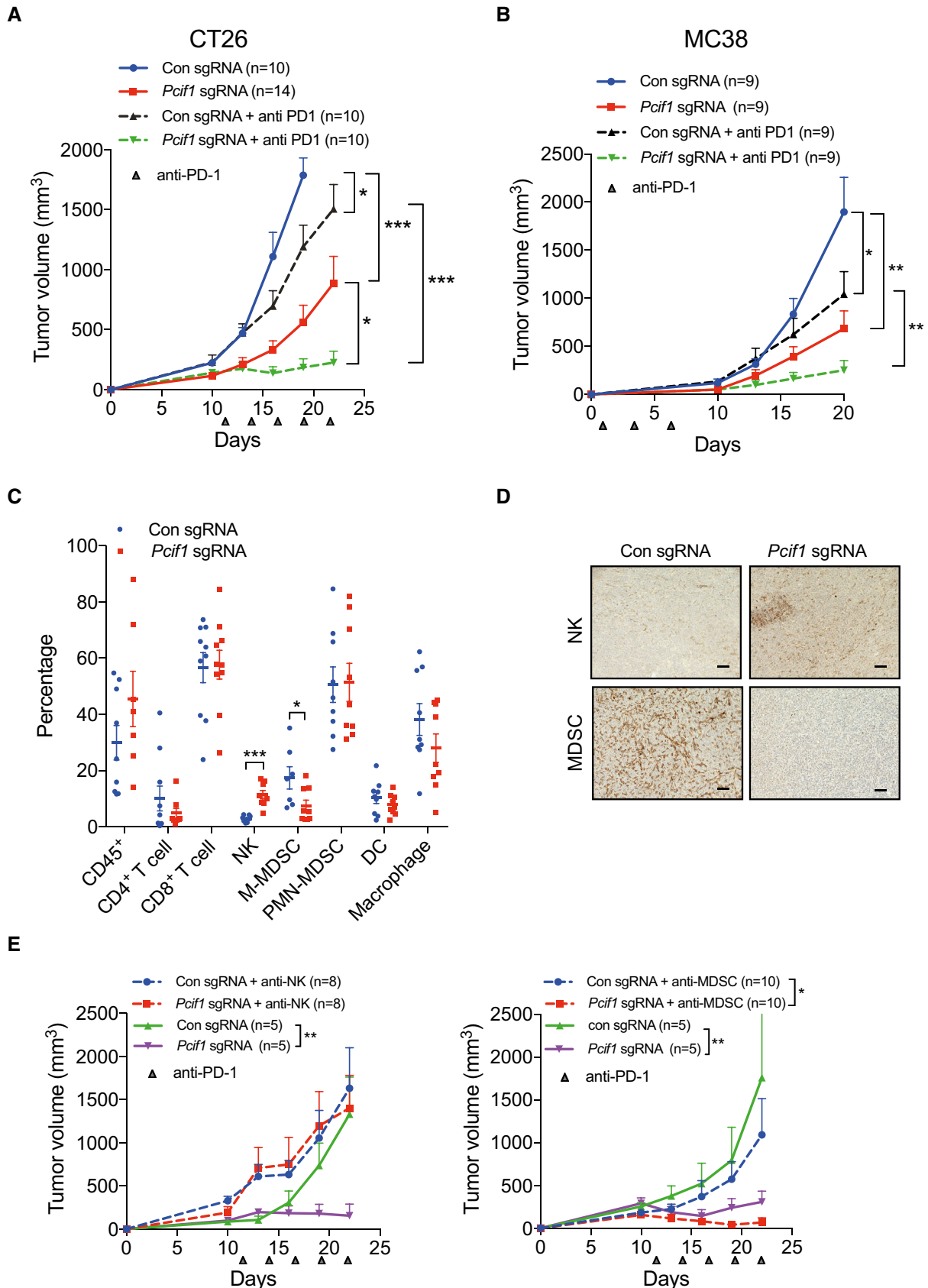


Figure 5.

**Figure 5. Depletion of *Pcif1* sensitizes mouse CRC to anti-PD-1 treatment.**

- A, B Growth of control and *Pcif1*-depleted CT26 (A) and MC38 (B) tumors in BALB/c and C57 BL/6 mice, respectively, untreated or injected intraperitoneally with 200  $\mu$ g anti-PD-1 antibody. *n*, number of mice. Data are the mean  $\pm$  SEM of the number of mice/group indicated on each panel. \**P* < 0.05, \*\**P* < 0.01, \*\*\**P* < 0.001 by Student's *t*-test.
- C Flow cytometric analysis of the percentage of total CD45+ lymphocytes, CD4+ T cells, CD8+ T cells, NK cells, MDSCs, DCs, and macrophages in extracts of control and *Pcif1*-depleted CT26 tumors as indicated. Each spot represents individual mice. Data are the mean  $\pm$  SEM of the number of mice/group as indicated. \**P* < 0.05; \*\*\**P* < 0.001 by Student's *t*-test.
- D Representative images of IHC staining of NK and MDSC cells in control and *Pcif1*-depleted CT26 tumors. *n* = 3 mice/group. Scale bars, 25  $\mu$ m.
- E Growth of control and *Pcif1*-depleted CT26 tumors in BALB/c mice injected with 200  $\mu$ g anti-PD-1 antibody with/without depleted of NK or MDSC cells as indicated. Data are the mean  $\pm$  SEM of the number of mice/group indicated on each panel. \**P* < 0.05, \*\**P* < 0.01 by Student's *t*-test.

BALB/c mice. Tumors formed by control and *Pcif1*-depleted CT26 cells showed no significant differences in the numbers of tumor-associated total tumor infiltrated CD45+ lymphocytes, CD4+ T cells, CD8+ T cells, polymorphonuclear myeloid-derived suppressor cells (PMN-MDSCs), dendritic cells (DCs), or macrophages (Figs 5C and EV4C–E). However, *Pcif1*-depleted tumors contained significantly higher numbers of NK cells and significantly lower numbers of mononuclear MDSCs (M-MDSCs) compared with control tumors (Fig 5C). Moreover, the same specific increase in NK cells and reduction in M-MDSCs were observed in *Pcif1*-depleted compared with control tumors formed by MC38 cells (Fig EV5A). Consistent with these findings, IHC staining of CT26 tumors indicated markedly higher staining with the NK cell marker anti-NK1.1 and lower staining with the MDSC marker anti-Ly6G/Ly6C compared with control tumors (Fig 5D). Given that NK cells and M-MDSCs promote and inhibit antitumor immunity, respectively, these findings suggest that alterations in the abundance of these cell types may play a role in the growth-suppressive effects of PCIF1 depletion. To assess this, we injected mice with anti-NK1.1 or anti-Ly6G/C antibodies twice weekly starting on day 5 after tumor cell inoculation to deplete the mice of NK cells or MDSCs, respectively. Notably, the tumor-suppressive effects of *Pcif1* knockout was completely reversed in mice depleted of NK cells, whereas enhanced response to immunotherapy by *Pcif1* loss was not abolished by MDSCs depletion (Fig 5E). These results are consistent with a crucial role for NK cells in mediating the antitumor effects of PCIF1 knockout.

### The mechanisms of *Pcif1* in modulating CRC tumor microenvironment during immunotherapy

Finally, we asked whether *Fos* activity might contribute to the additive effects of *Pcif1* depletion on anti-PD-1 treatment of *Pcif1*-depleted CRC tumors. *Fos* mRNA levels and protein levels were reduced in *Pcif1*-depleted CT26 tumors compared with control tumors excised from anti-PD-1-treated mice (Figs 6A and EV5B). Moreover, decreased m<sup>6</sup>Am levels of *Fos* were detected in *Pcif1* null tumors by m<sup>6</sup>Am-exo-qPCR experiments as well (Fig 6B), indicating that *Pcif1* continues to regulate *Fos* under immunotherapy. Since TGF- $\beta$  is closely connected to immunotherapy, where exposure to TGF- $\beta$  ligand limits the activity of NK cells, while TGF- $\beta$  signaling suppression preserves highly activated NK cells to kill cancer cells (Otegbeye et al, 2018; Itatani et al, 2019). Therefore, we continued to assess the expression of TGF $\beta$ s using qRT-PCR analysis. Evaluation of Tgfb expression showed that Tgfb1-3 were all downregulated in *Pcif1*-depleted tumors (Fig EV5C), and, interestingly, this was accompanied by a significant reduction in intratumoral levels, but not serum levels, of Tgfb1-3 secretion (Figs 6C and EV5D). To

further investigate if the mechanism of enhanced immunotherapy response of *Pcif1*-deficient tumors relies on the decreased *Fos*, we overexpressed *Fos* in *Pcif1*-depleted and parental CT26 cells (Fig EV5E), and then compared the tumor growth of these cell with *Pcif1* knockout tumors only under immunotherapy. Mice bearing *Pcif1*-depleted tumors with *Fos* overexpression reversed the observed effects on *Pcif1* null tumor growth (Fig 6D). Furthermore, the reduced production of TGF- $\beta$ s from *Pcif1* null tumors was restored as well (Fig 6E). Accordingly, *FOS* overexpression alone significantly increased tumor size (Fig 6D) and TGF $\beta$ s' secretion compared to control (Fig 6E). Taken together, these results suggest that *Pcif1*-mediated regulation of the tumor response to anti-PD-1 antibody therapy is mediated via m<sup>6</sup>Am modification of *Fos* mRNA, *Fos*-regulated TGF- $\beta$  production, and recruitment/retention of NK cells in the TME.

In order to obtain further mechanistic insight into how *Pcif1* depletion remodels the TME, we performed RNA-seq in *Pcif1*-depleted CT26 depleted and control tumors with anti-PD-1 treatment. Our RNA-seq analysis identified 560 genes were upregulated and 514 genes were downregulated in *Pcif1* depleted tumors compared with control tumors (Fig 6F; Dataset EV4). According to Gene Ontology (GO) classification, these genes were enriched in the pathways associated with innate immune response, response to cytokine, interferon-gamma (IFN- $\gamma$ ) signaling and regulation of cell death, cellular proliferation, migration, adhesion etc. (Fig 6G). Given that IFN- $\gamma$  signaling is a critical contributor to adaptive resistance mechanisms of the checkpoint blockade therapy and has substantial effects on antitumor immune responses (Sharma et al, 2017), upregulated genes involved in the interferon  $\gamma$  pathway (*Irf1*, *Stat1*, *Stat2*, *Jak2*, *Ciita*, *Ifitm3*, *Gbp6*, *Irgm1* and *Faslg*) were further confirmed by qRT-PCR. We found that *Irf1*, *Stat1*, *Ciita* and *Ifitm3* are the common upregulated genes in both *Pcif1*-depleted CT26 and MC38 tumors compared to control (Fig EV5F and G), suggesting that *Pcif1* depletion is involved in enhancing IFN- $\gamma$  response. Further m<sup>6</sup>Am-exo-qPCR experiments showed that *Ifitm3* and *Stat1* were m<sup>6</sup>Am-modified genes by *Pcif1* (Fig 6H). Above findings support that *Ifitm3* and *Stat1* are the specific targets of *Pcif1* under immunotherapy. We next investigated whether depleting IFN- $\gamma$  influence the effect of *Pcif1* deletion on tumor growth during immunotherapy. To address this question, we treated the BALB/c mice with anti-IFN- $\gamma$ -antibody during anti-PD1 treatment of control sgRNA and *Pcif1* sgRNA tumors. Our results showed that blocking of IFN- $\gamma$  reversed the inhibition of tumor growth by loss of *Pcif1* under immunotherapy (Fig EV5H). These results suggest that IFN- $\gamma$  is essential to suppress tumor growth by *Pcif1* depletion during anti-PD-1 treatment. Since IFN- $\gamma$  and TNF $\alpha$  as two of the most potent effector cytokines secreted by NK cells play a key role in antitumor

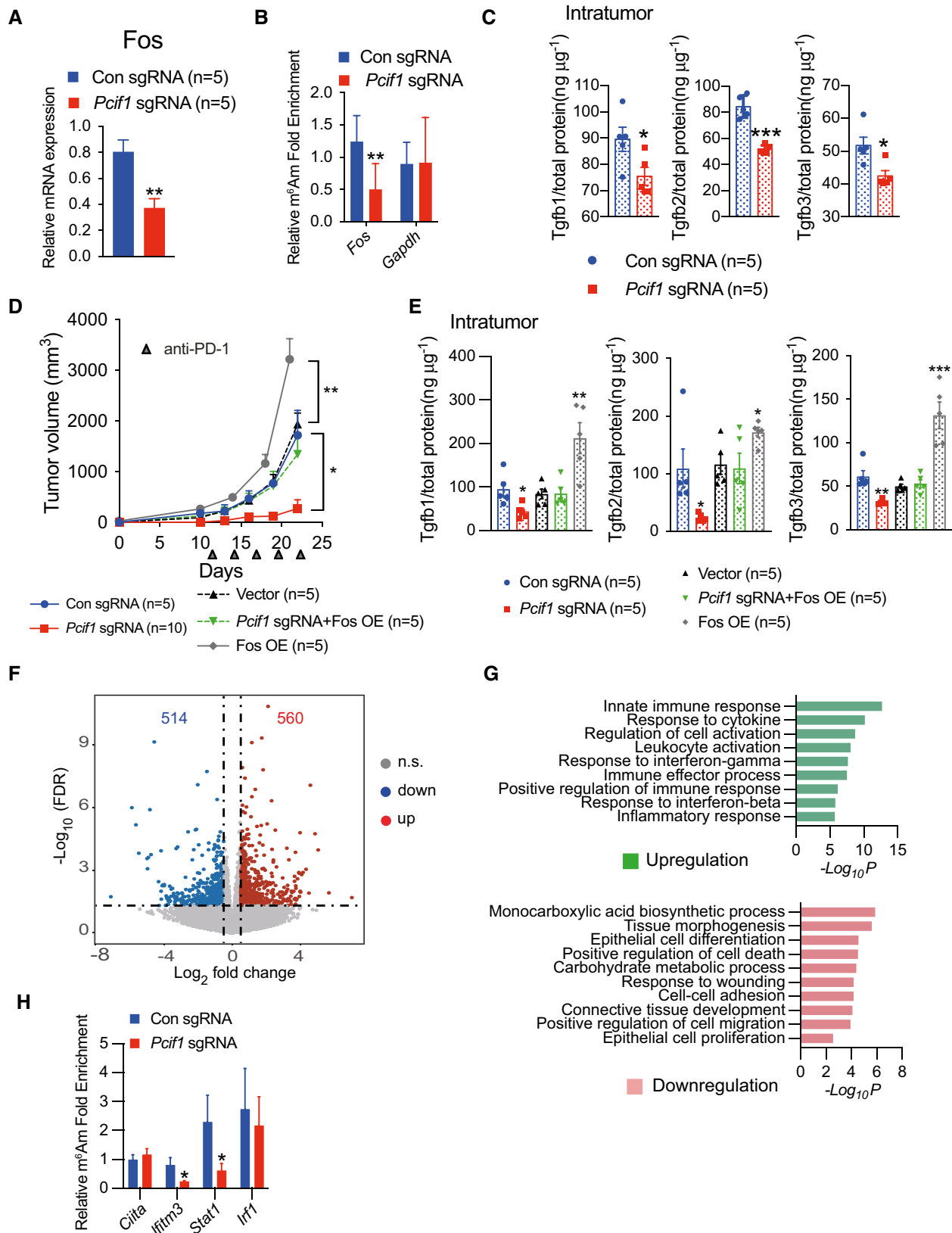


Figure 6.

**Figure 6. Pcf1-depletion alters the CRC tumor microenvironment during anti-PD-1 immunotherapy.**

- A qRT-PCR analysis of *Fos* mRNA expression in control and *Pcf1*-depleted CT26 tumors after anti-PD-1 antibody injection. Data are the mean  $\pm$  SEM of  $n = 5$ . \*\* $P < 0.01$  by Student's *t*-test.
- B  $m^6Am$ -exo-qPCR analysis of  $m^6Am$  enrichment in *Fos* mRNA in control and *Pcf1*-depleted CT26 tumors. *Gapdh* served as a negative control. Data are the mean  $\pm$  SEM of  $n = 3$ . \*\* $P < 0.01$  by Student's *t*-test.
- C ELISA quantification of *Tgfb1-3* secretion levels in tumor extracts from BALB/c mice injected with control and *Pcf1*-depleted CT26 cells. Data are the mean  $\pm$  SEM of  $n = 5$ . Symbols represent individual mice. \* $P < 0.05$ , \*\*\* $P < 0.001$  by Student's *t*-test.
- D Tumor growth with the indicated gene edited CT26 cells in BALB/c mice treated with anti-PD-1 antibody.  $n$ , mouse number. Data are the mean  $\pm$  SEM of the indicated mice in each group. \* $P < 0.05$ , \*\* $P < 0.01$  by Student's *t*-test.
- E Production of *Tgfb1-3* was measured by ELISA from the indicated tumors. Data are the mean  $\pm$  SEM of  $n = 5$ . Symbols represent individual mice. \* $P < 0.05$ , \*\* $P < 0.01$ , \*\*\* $P < 0.001$  by Student's *t*-test.
- F Volcano plot of differentially expression genes analyzed using DESeq2 in *Pcf1*-depleted tumors compared with control. Significantly up or downregulated genes are plotted in red and blue points, respectively. n.s, nonsignificant.
- G Meta-enrichment analysis summary for the significant up and down-regulated genes identified as *Pcf1* targets in CT26 tumor with PD-1 treatment.
- H  $m^6Am$  enrichment in the indicated mRNA was assessed in control and *Pcf1*-depleted CT26 tumors by  $m^6Am$ -exo-qPCR. Data are the mean  $\pm$  SEM of  $n = 3$ . \* $P < 0.05$  by Student's *t*-test.

activity (Paul & Lal, 2017), therefore, we then assessed the production of IFN- $\gamma$  and TNF $\alpha$  in both mouse serum and tumors by ELISA. Our results suggested that compared to control, the production of IFN- $\gamma$  and TNF $\alpha$  was significantly increased in mouse tumors with *Pcf1* depletion, whereas no differences in serum were observed (Fig EV5I). Thus, these results indicated the increased production of IFN- $\gamma$  and TNF $\alpha$  in the TME also contributed to the enhanced efficacy of immunotherapy in *Pcf1*-depleted tumors. Collectively, our findings revealed a context depended mechanisms of PCIF1 in CRC tumorigenesis and response to anti-PD-1 treatment. In summary, the PCIF1-FOS-TGF- $\beta$  axis regulates CRC tumors growth, whereas, during the immunotherapy, the *Pcf1*-Fos-TGF- $\beta$  and *Pcf1*-Stat1/Ifitm3-IFN- $\gamma$  mechanisms play essential roles in the interactions between the tumor and immune system (Fig 7H).

#### Formulation and characterization of LNP-CMsiRNA as advanced tools for clinical translational application

Our results demonstrated that loss of  $m^6Am$  methyltransferase PCIF1 inhibits tumor malignancy and potentiates anti-PD-1 response during immunotherapy. In order to investigate the clinical translational potential of our findings, we developed efficacious nanoparticle-mediated siRNA delivery system. To obtain an effective PCIF1 silencing *in vivo*, we chemically modified siRNAs (CMsiRNAs) to enhance their loading into RISC (RNA-induced silencing complex) assembly, stability, lipophilicity, and cell permeability. RNA sequences were modified with 5'-end phosphorylation, 2'-*O*-methyl U, and conjugated with cholesterol at the 3' end (Fig 7A). PCIF1 silencing activities of modified siRNAs were analyzed by transfecting cells with varying amounts of siRNAs. Compared to control, PCIF1 expression was effectively reduced by the two designed siRNAs at the both mRNA and protein levels in a dose-dependent manner (Fig 7B and C). Further, the effect of *PCIF1* siRNA on cell survival was determined, and the results showed that PCIF1 siRNAs significantly inhibited cellular viability (Fig 7D). We next formulated siRNAs in LNPs at varying ratios from 16:1 to 4:1 (weight ratio of LNP: siRNA) for size analysis using the Zetasizer system. The estimated mean diameter of the LNP-siRNA formulations with LNP: siRNA weight ratio at 8:1 was 125 nm, and this ratio was selected as the formulation for *in vivo* LNP-siRNA administrations (Fig 7E). To further assess the efficiency of PCIF1 silencing by LNP-siRNA formulation *in vivo*, 1 mg/kg of LNP-siRNAs were

injected intratumorally into the athymic nude mice twice a week. Our results showed that the tumor size was significantly reduced in mice treated with LNP-*PCIF1* siRNAs as compared with control siRNA (Fig 7F), and efficient silencing of PCIF1 in tumors was also observed by immunoblotting (Fig 7G). Altogether, these results suggest a new possibility to improve therapeutic methods for patients with CRC through the suppression of PCIF1 using siRNA therapy.

## Discussion

In the present study, we sought to determine whether  $m^6Am$  RNA modification by PCIF1 plays a role in CRC growth and response to ICB. The results reveal several new findings: First, PCIF1 is upregulated in CRC and correlates inversely with survival, suggesting that it plays an oncogenic role. Second, PCIF1 regulates the expression of genes associated with pathways involved in tumor malignancy and controls those cell behaviors *in vitro* and *in vivo*. Third, PCIF1-mediated deposition of  $m^6Am$  regulates FOS mRNA stability and transcription of TGF- $\beta$ . Fourth, *Pcf1* regulates recruitment and/or retention of NK cells and *Tgfb1-3*, IFN- $\gamma$ , and TNF- $\alpha$  levels in the tumor microenvironment. Finally, downregulation of *Pcf1* significantly increases the sensitivity of CRC tumors to anti-PD-1 therapy *in vivo* through regulating *Pcf1*-mediated Fos-Tgf- $\beta$  and Stat1/Ifitm3-IFN- $\gamma$  axes, establishing this methyltransferase as a contributor to CRC resistance to this therapy. Overall, our study demonstrates a key role for PCIF1 and the  $m^6Am$  modification in regulating the balance between pro- and anti-proliferative conditions in the CRC TME and the response to anti-PD-1 immunotherapy.

Our findings suggest that components of the PCIF1-FOS-TGF- $\beta$  pathway may serve as therapeutic targets not only for cancer therapy directly but also as modulators of ICB responses. The promoting role of  $m^6Am$  in CRC development demonstrated in this study indicated the abolishment of this modification could be beneficial to cancer treatment. Here, we developed a LNPs packaging system for intratumoral chemically modified siRNA delivery and a significantly reduced tumor growth was found in mice treated with LNP-*PCIF1* siRNA as compared to control. These results provide a proof-of-concept for siRNA-mediated silencing of target genes for potential clinical applications. Besides, it has been reported that the loss of PCIF1 in mice does not affect viability or fertility (Pandey et al, 2020), thus, we are expecting the development of PCIF1

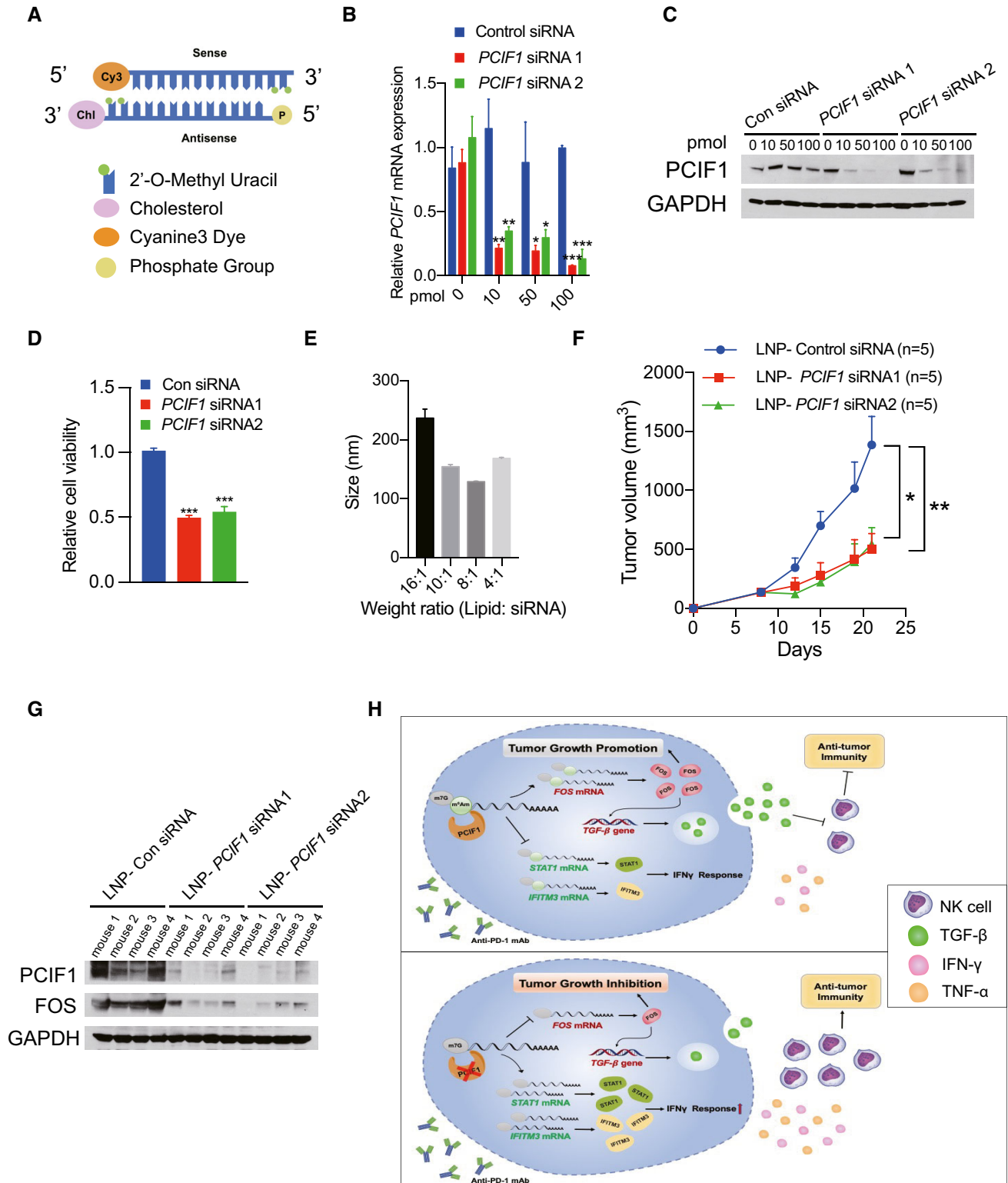


Figure 7.

inhibitor could open-up the possibility to enhance the performance of immunotherapy for CRC through the suppression of m<sup>6</sup>Am modification. Similarly, inhibitors of methyltransferase METTL3 have

been recently developed to treat myeloid leukemia (Bedi *et al.*, 2020; Yankova *et al.*, 2021). Taken together, our study delineates the role of m<sup>6</sup>Am in both CRC tumors and its response to immunotherapy,

**Figure 7. On-target efficacy of LNP-siRNA *in vitro* and *in vivo*.**

- A Structures of siRNAs utilized in this study.
- B mRNA expression of *PCIF1* was quantified by qRT-PCR in the HCT116 cells transfected with gradient amount of control and *PCIF1* siRNAs. Data are the mean  $\pm$  SD of  $n = 3$  biological replicates. \* $P < 0.05$ , \*\* $P < 0.01$ , \*\*\* $P < 0.001$  by Student's *t*-test.
- C Western blot analysis of *PCIF1* in HCT116 cells with control and *PCIF1* siRNAs. GAPDH served as a loading control.
- D Cell viability assays were performed in the HCT116 cells transfected with 100 pmol control and *PCIF1* siRNAs. Data are the mean  $\pm$  SD of  $n = 3$  biological replicates. \*\*\* $P < 0.001$  by Student's *t*-test.
- E Size of LNP-siRNA formulations were analyzed by Zetasizer. Data are the mean  $\pm$  SD of  $n = 3$  biological replicates.
- F Tumor growth of HCT116 cells treated with 1 mg/kg control and *PCIF1* LNP-siRNAs starting on day 9 and mice were intratumorally treated twice a week. Data are the mean  $\pm$  SEM of  $n = 5$  mice/group. \* $P < 0.05$ , \*\* $P < 0.01$  by Student's *t*-test.
- G Immunoblots of *PCIF1* and *FOS* were carried out from the indicated tumors in four replicates with GAPDH as a loading control.
- H Schematic of the proposed function of *PCIF1*-mediated m<sup>6</sup>Am modification in CRC.

Source data are available online for this figure.

which provides broader mechanistic insight for our understanding and the potential clinical application value of RNA modification in cancer patients' treatment.

## Materials and Methods

### Immunohistochemical staining

Human colorectal cancer tissues were obtained from US Biomax. The staining procedure for paraffin-embedded mouse and human tissues were as previously described (Mu *et al*, 2018). Tissue staining was semi-quantitatively scored on a 0–9 scale by multiplying the score for the proportion of positively stained tumor cells (0, < 10%; 1, 10–25%; 2, 26–50%; 3, > 50%) by the staining intensity score (0–3) as previously defined (Wang *et al*, 2021). For the comparison of low/high *PCIF1* expression and patient survival, overall survival was defined as the time between date of diagnosis and death. Primary antibodies used in IHC include anti-*PCIF1* (Invitrogen, PA5-61996), anti-*FOS* (Abcam, ab222699), anti-Ki-67 (Cell Signaling Technology, 12202T), anti-Ly-6G/Ly6C (Invitrogen, 14-5931-81), and anti-NK1.1 (Invitrogen, MA1-70100).

### Western blot analysis

Cells or tumor tissues were lysed in RIPA buffer supplemented with protease inhibitors (Life Technologies, 87786), sonicated, and centrifuged. Protein concentrations in the supernatants were measured using a BCA protein assay kit (Bio-Rad). Total protein samples were resolved on 4–12% NuPAGE Bis-Tris or Tris-Glycine gels (Fisher Scientific) and transferred to PVDF membranes (Bio-Rad). Membranes were blocked with 5% (w/v) nonfat dry milk in PBS and incubated with primary antibodies against GAPDH (Proteintech, HRP-60004), *PCIF1* (Proteintech, 16082-1), *FOS* (Abcam, ab222699), *TGFBI* (Abcam, ab179695), *TGFBI2* (Proteintech, 19999-1-AP), *TGFBI3* (Proteintech, 18942-1-AP), tubulin (Santa Cruz Biotechnology, sc-5286), or lamin A/C (Santa Cruz Biotechnology, sc-6215) overnight at 4°C. Membranes were then incubated with HRP-conjugated secondary antibodies for 15 min at 25°C (Thermo Scientific, Pierce Fast Western Blotting Blot Kit). Protein bands were visualized using the enhanced chemiluminescence (ECL) detection system (Thermo Scientific) followed by imaging of X-ray film (GeneSee Scientific, 30-100).

### RNA purification and quantitative reverse-transcription PCR (qRT-PCR)

RNA was extracted from cultured cells using Quick-RNA Miniprep Kit (Zymo Research, R1055) and from fresh mouse tumors using Direct-zol RNA MiniPrep Kit (Zymo Research, 11-331) according to the manufacturer's instructions. Aliquots of 1  $\mu$ g RNA were reverse-transcribed using an iScript cDNA Synthesis Kit (Bio-Rad, 1708841), and qPCR was performed with SsoAdvanced Universal SYBR Green PCR SuperMix (Bio-Rad, 1725270) on an LightCycler480 PCR system. All qPCR primers are listed in Table EV1.

### Immunofluorescence microscopy

Cells were grown in 24-well tissue culture plates, washed with PBS, fixed with 4% formaldehyde for 10 min, permeabilized with PBS containing 0.5% Triton X-100 for 10 min, blocked with 10% goat serum for 60 min, and incubated with primary anti-*PCIF1* antibody (Proteintech, 16082-1) for 1 h. The cells were then washed, incubated with a secondary antibody conjugated to anti-Rabbit Alexa Fluor 488 dye (Thermo Scientific, A-11034) for 1 h, and counter-stained with 4',6-diamidino-2-phenylindole (DAPI) for 10 min.

### Cell culture and viral infection

The normal human colon cell line CCD841CoN (CRL-1790) and human CRC cell lines HCT116 (CCL-247), DLD-1 (CCL-221), WiDr (CCL-218), LS123 (CCL-255), LS174T (CL-188), and HT29 (HTB-38) were purchased from American Type Culture Collection (ATCC; Manassas, VA). The murine CRC cell lines CT26 (CRL-2638) and MC38 (ENH204-FP) were obtained from the ATCC and Kerfast, Inc., respectively. 293T (CRL-3216) cells were obtained from ATCC. Cells were grown in EMEM (ATCC), DMEM, or RPMI (Gibco) supplemented with 10% fetal bovine serum (Gibco) and were maintained at 37°C in a 5% CO<sub>2</sub> atmosphere according to ATCC's culture methods, respectively.

For lentiviral production, 293T cells were co-transfected with the packaging plasmids psPAX2 and pMD2.G, CRISPRV2, and the indicated sgRNAs in 10 cm dishes using Lipofectamine (Life Technologies, 11668027) in Opti-MEM medium (Gibco). The medium was replaced with fresh complete DMEM after 4–6 h, and the cells were incubated at 37°C for an additional 48 h. Culture supernatants were then removed and used to infect cells by spin transduction. SgRNAs for targeting human genes were *PCIF1*-sgRNA1:

CGGTTGAAAGACTCCCGTGG; *PCIF1*-sgRNA2: TTCGGCGTGGGCCTCTACGA; *PCIF1*-sgRNA3: GATCCGTTTGACGTACTCCA; *PCIF1*-sgRNA4: ATTCACCAACCAGTCCCTGT. *FOS*-sgRNA1: CTGCAGC-CAAATGCCGAAC; *FOS*-sgRNA2: CTTCGTCTTACCTACCCCG; and *FOS*-sgRNA3: AACCGCCACGATGATGTTCT. SgRNAs for targeting mouse genes were: *Pcif1*-sgRNA1: TGAAGCTCCGCCAGCACTA C; *Pcif1*-sgRNA2: CACGTCTGCTGACCCAGCA; *Pcif1*-sgRNA3: GC TTCAAGATGAGCTGCGAG; and *Pcif1*-sgRNA4: CTCTGAGAGCTG TCGCTTC.

### Transwell invasion assay

Cells were plated at  $2 \times 10^5$ /well into Transwell chambers containing 8- $\mu$ m pore size filters (BD Biosciences) in serum-free medium, and the assay was performed as previously described (Wang et al, 2021). After 24 h, invaded cells were stained with crystal violet solution (bioWORLD, 30430001-1) and enumerated under a light microscope.

### Wound healing and migration assay

Cells at  $5 \times 10^4$  cells/ml were added to Culture-Insert 3 wells (Ibidi, 80366) in complete medium according to the manufacturer's instructions. Briefly, after cell attachment (12–24 h), the culture-insert 3 well was gently removed by using sterile tweezer and the dish was filled with cell medium. The dishes were subsequently washed with cell medium and cells were analyzed using a microscope at 0 and 48 h.

### Cell adhesion assay

DMEM containing fibronectin (10  $\mu$ g/ml; R&D Systems, Minneapolis, MN) was added to 48-well plates and incubated at 4°C for 12 h. The wells were washed and  $5 \times 10^4$  cells/well were added and the plates were incubated for 15 min at 37°C. Nonadherent cells were then rinsed away with PBS, and adherent cells were fixed with 4% paraformaldehyde, stained with 0.1% crystal violet solution, and enumerated.

### Colony formation assay

Aliquots of  $1 \times 10^3$  cells/well were added to 6-well plates and incubated for 14 days. Cells were fixed with 4% paraformaldehyde, stained with 0.1% crystal violet solution, and photographed. Colonies, defined as foci contained  $\geq 50$  cells, were enumerated.

### Animal experiments

Protocols were approved by the Institutional Animal Care and Use Committee at the University of California, San Diego, and studies were performed in accordance with Committee guidelines. BALB/c and C57BL/6J mice at 6–8 weeks of age and athymic nude mice at 4–5 weeks of age were purchased from The Jackson Laboratory. CT26 or HCT116 cells with two independent control and *PCIF1*/*FOS* sgRNAs subjected to the indicated treatments were resuspended at  $2 \times 10^6$  in 200  $\mu$ l of 1:1 PBS: Matrigel (Corning) and injected subcutaneously into the flanks of BALB/c mice (CT26) or athymic nude mice (HCT116). Mice were injected intraperitoneally with 200  $\mu$ g (10 mg/kg) of anti-PD-1 antibody (Bio X Cell, clone 29F.1A12) on

days 11, 14, 17, 20, and 23 after tumor injection as previously described (Wang et al, 2020). MC38 cells with two independent control and *Pcif1* sgRNAs subjected to the indicated treatments were resuspended at  $5 \times 10^5$  in PBS and injected into the flanks of C57BL/6J mice. The mice were injected intraperitoneally with 200  $\mu$ g (10 mg/kg) anti-PD-1 antibody on days 1, 4, and 7 after tumor injection.

For *in vivo* depletion of NK cells and MDSCs, CT26 tumor-bearing mice were injected intraperitoneally with 200  $\mu$ g (10 mg/kg) of anti-NK1.1 (Bio X Cell, clone PK136) or anti-Ly6G/Ly6C (Bio X Cell, clone RB6-8C5) antibodies twice weekly starting on day 5. Tumor sizes were measured on the indicated days and tumor volumes were calculated as: volume ( $\text{mm}^3$ ) = (long diameter  $\times$  short diameter<sup>2</sup>)/2. For the *in vivo* IFN- $\gamma$  blocking experiments, BALB/c mice bearing the control and *Pcif1*-depleted tumors were treated i.p. with 200  $\mu$ g (10 mg/kg) of anti-IFN- $\gamma$  antibody (Bio X Cell, Clone: XMG1.2) every 2 days starting on day 7 and injected i.p. with 200  $\mu$ g (10 mg/kg) of anti-PD1 antibody as indicated.

### MTS proliferation assay

$2 \times 10^3$  cells were seeded into each well of 96-well plates and then processed at the indicated time using a CellTiter Aqueous One Solution Cell Proliferation Assay Kit (Promega, G3580) according to the manufacturer's instructions. Absorbance at 490 nm was recorded.

### Flow cytometry

Control and *Pcif1*-depleted mice tumors were weighed, diced mechanically, and then digested with 2 mg/ml collagenase P (Sigma-Aldrich) and 50  $\mu$ g/ml DNase I (Sigma-Aldrich) for 30 min at 37°C. The cells were filtered through a 70- $\mu$ m cell strainer and stained as previously described (Wang et al, 2020) with antibodies against CD45 (clone 30-F11), CD3e (clone 145-2C11), NK1.1 (clone PK136), CD4 (clone RM4-5), CD8 (clone 53-6.7), MHC class II (clone M5/114.15.2), CD24 (clone M1/69), F4/80 (BM8), and CD11b/Ly-6C/Ly-6G (Mouse MDSC Flow Cocktail 2, clones M1/70, 1A8, and HK1.4), all from BioLegend.

### RNA-seq

RNA was extracted from *PCIF1*-depleted and control HCT116 cells (four biological replicates per group) using Quick-RNA Miniprep Kit (Zymo Research, R1055). RNA-seq library preparation and sequencing were performed at the IGM Genomics Center, UCSD, using an Illumina HiSeq 4000. Single-end reads were trimmed using cutadapt (v1.18) and mapped to human genome (hg38) through HISAT2 (v2.1.0). Transcripts were quantified via HTSeq (0.11.2), and differentially expressed genes were then determined by DESeq2. Genes with a *P* value < 0.05 and fold change < 1 were considered down-regulated and selected for further analysis.

### m<sup>6</sup>Am-exo-seq and m<sup>6</sup>Am-exo-qPCR

m<sup>6</sup>Am-exo-Seq was performed according to previously described protocols (Sendinc et al, 2019). Briefly, mRNA was purified from control and *PCIF1*-depleted HCT116 cells using a Magnetic mRNA Isolation Kit (New England Biolabs, S1550S). mRNA was then

fragmented with a Fragmentation Reagents Kit (Invitrogen, AM8740), phosphorylated with T4 PNK (NEB, M0201S), and treated with Terminator 5'-Phosphate-Dependent Exonuclease (Lucigen) to remove phosphorylated transcripts. Lastly, Cap-Clip (CellScript) was used to remove capped transcripts. A sample equivalent to 10% of the 5'-uncapped mRNA fragments was reserved as input, and the remainder was immunoprecipitated with anti-m<sup>6</sup>A antibody (Abcam, ab151230). Library generation and sequencing were performed at IGM Genomics core, UCSD on an Illumina NovaSeq 6000.

For m<sup>6</sup>Am-exo-qPCR, mRNA was extracted from freshly excised control and Pcf1-depleted tumors and processed using the procedures described above. Reserved input and anti-m<sup>6</sup>Am immunoprecipitated samples were reverse-transcribed and analyzed by qPCR as described above.

### m<sup>6</sup>Am-exo-seq analysis

Paired-end reads generated from the m<sup>6</sup>Am-exo-seq data were trimmed by cutadapt and then mapped to the human genome (hg38) using HISAT2. Reads that fell within 100 bp upstream/downstream of TSS sites were considered TSS reads, which were then quantified by featureCount in Rsubread package and normalized by sequencing depth. For each gene, normalized TSS reads from immunoprecipitates or input samples from control or PCIF1-depleted cells were subjected to a hypergeometric test, and the fold-change enrichment was defined as  $\text{fold change} = \frac{KO_{PCIF1} IP_{KO_{PCIF1}} Input}{WT IP_{WT} Input}$ . Genes with  $P < 0.05$  and fold change  $< 1$  were defined as cap-m<sup>6</sup>Am-modified genes.

### HPLC-MS/MS

mRNA was purified from control and PCIF1-depleted cells using a Magnetic mRNA Isolation Kit (New England Biolabs, S1550S) according to the manufacturer's protocol. Aliquots of 0.5 µg mRNA were de-capped with 1 U Cap-Clip (CellScript) at 37°C for 1 h and digested with 0.5 U of nuclease P1 (Sigma) at 37°C for 2 h. Ammonium bicarbonate and alkaline phosphatase (Sigma) were added and the mixture was incubated at 37°C for 2 h. The samples were then filtered (0.22-µm pore, Millipore) and analyzed by LC-MS/MS as previously described (Li et al, 2020; Huff et al, 2021).

### mRNA stability

mRNA stability was assessed as previously reported (Wei et al, 2018). In brief, PCIF1-depleted and control HCT116 and HT29 cells were treated with 5 µg/ml actinomycin D (Alfa Aesar, AAJ67160XF) for 0, 30, 60, or 120 min, and FOS mRNA levels were then quantified by qRT-PCR. Primers are listed in Table EV1.

### Cytokine ELISA

Mouse serum samples and CT26 tumor extracts were prepared as described previously (Wang et al, 2020). The secretions of Tgfb1, Tgfb2, Tgfb3, IFN-γ, and TNFα were quantified using a TGF beta-1 Human/Mouse ELISA Kit (Fisher Scientific, 88-8350-22), a mouse TGFβ2 ELISA Kit (Aviva Systems Biology, OKEH00309), a Tgfb3 mouse ELISA Kit (Boster Biological Technology, EK1104), an IFN-γ

mouse ELISA Kit (Fisher Scientific, 88-7314-22), and a TNFα mouse ELISA Kit (Fisher Scientific, 88-7324-22), respectively, according to the manufacturers' protocols.

### Formulation of LNP-siRNAs

The LNP-siRNA was formulated using previous protocols as described (Jayaraman et al, 2012). Briefly, LNPs were formed by mixing lipids (Selleckchem, S6683), 1, 2-distearoyl-sn-glycero-3-phosphocholine (DSPC) (Avanti Polar Lipids, 850365p-200mg), cholesterol (Sigma, C3045), and DMG-PEG2000 (Avanti Polar Lipids, 880151p-1g) at a molar ratio of 50:10:38.5:1.5 in ethanol. siRNA solutions were diluted in 50 mM sodium citrate (pH = 4) such that the final weight ratio of lipid: siRNA was achieved from 16:1 to 4:1, accordingly, the mixture was incubated for 15 min at 37°C to encapsulate the siRNAs. LNP-siRNAs were diluted in PBS and analyzed further. siRNAs used in this study are listed below:

control siRNA: 5'-U.U.G.U.A.G.G.C.C.A.G.C.U.G.U.G.A.G.U.A.G-3' (Sense);

5'-C.U.A.C.U.C.A.C.A.G.C.U.G.G.C.C.U.A.C.A.A-3' (Antisense).

PCIF1 siRNA1: 5'-U.U.A.U.A.C.C.G.G.A.U.G.C.A.G.A.C.C.A.C.G-3' (Sense);

5'-C.G.U.G.G.U.C.U.G.C.A.U.C.C.G.G.U.A.U.A.A-3' (Antisense).

PCIF1 siRNA2: 5'-A.U.G.A.C.A.G.C.A.U.U.G.G.U.C.U.G.G.A.U.G-3' (Sense);

5'-C.A.U.C.C.A.G.A.C.C.A.A.U.G.C.U.G.U.C.A.U-3' (Antisense).

### Cell viability assay

$5 \times 10^3$  cells were seeded into each well of 96-well plates and performed the experiment using a CellTiter-Glo<sup>®</sup> Luminescent Cell Viability Assay kit (Promega, G7570) according to the manufacturer's instructions. Briefly, a volume of CellTiter-Glo Reagent equal to the volume of cell culture medium present in each well was added and mixed for 2 min. After 10 min, luminescence was recorded.

### Statistical analysis

Data were analyzed using Prism 5.0 software (GraphPad) and are presented as the mean ± standard deviation (SD) or standard error (SEM) as indicated.  $P$  values were determined using Student's  $t$ -test and were considered to be significant at  $< 0.05$ .

## Data availability

RNA-seq and m<sup>6</sup>Am-exo-seq data were deposited at the Gene Expression Omnibus database (<https://www.ncbi.nlm.nih.gov/geo/>) under accession number GSE175803.

**Expanded View** for this article is available [online](#).

### Acknowledgments

We thank Dr. Kristen Jepsen of the Institute of Genomic Medicine at UCSD for help with HTSeq, Dr. Neal Sekiya and Ms. Tara Rambled at the Center for AIDS Research at UCSD for flow cytometry analysis, Dr. M. Valeria Estrada at the Biorepository and Tissue Technology Shared Resource at UC San Diego Moores Cancer Center for assistance with histology and immunohistochemistry, and



members of the Rana lab for helpful discussions and advice. We also thank Ye Wang (University of California, Los Angeles) for help with the m<sup>6</sup>A-exo-seq data analysis and Dr. Yong Cheng at UCSD for assistance in LNP-siRNAs size analysis. This publication includes data generated at the UC San Diego IGM Genomics Center utilizing an Illumina NovaSeq 6000 that was purchased with funding from a National Institutes of Health SIG grant (#S10 OD026929). This work was supported in part by UCSD and grants from the National Institutes of Health (CA177322, CA030199, AI125103, DA046171).

### Author contributions

**Lingling Wang:** Formal analysis; validation; investigation; methodology; writing—original draft. **Lujing Wu:** Validation. **Zhouting Zhu:** Validation. **Gwendolyn Michelle Gonzalez:** Formal analysis; methodology. **Yinsheng Wang:** Formal analysis; methodology. **Tariq M Rana:** Conceptualization; formal analysis; supervision; funding acquisition; investigation; methodology; project administration; writing—review and editing.

### Disclosure and competing interests statement

TMR is a co-founder and has equity interest in Gibraltar Sciences, a company dedicated to developing targeted molecular and immunotherapies for untreatable cancers. The terms of this arrangement have been reviewed and approved by the University of California, San Diego in accordance with its conflict of interest policies.

## References

- Akichika S, Hirano S, Shichino Y, Suzuki T, Nishimasu H, Ishitani R, Sugita A, Hirose Y, Iwasaki S, Nureki O (2019) Cap-specific terminal N<sup>6</sup>-methylation of RNA by an RNA polymerase II-associated methyltransferase. *Science* 363: eaav0080
- Barbieri I, Tzelepis K, Pandolfini L, Shi J, Millán-Zambrano G, Robson SC, Aspris D, Migliori V, Bannister AJ, Han N (2017) Promoter-bound METTL3 maintains myeloid leukaemia by m<sup>6</sup>A-dependent translation control. *Nature* 552: 126–131
- Bedi RK, Huang D, Eberle SA, Wiedmer L, Caffisch A, Ślędek P (2020) Small-molecule inhibitors of METTL3, the major human epitranscriptomic writer. *ChemMedChem* 15: 744–748
- Boulias K, Toczyłowska-Socha D, Hawley BR, Liberman N, Takashima K, Zaccara S, Guez T, Vasseur J-J, Debart F, Aravind L (2019) Identification of the m<sup>6</sup>A methyltransferase PCIF1 reveals the location and functions of m<sup>6</sup>A in the transcriptome. *Mol Cell* 75: 631–643.e8
- Calon A, Lonardo E, Berenguer-Llgero A, Espinet E, Hernando-Momblona X, Iglesias M, Sevillano M, Palomo-Ponce S, Tauriello DV, Byrom D et al (2015) Stromal gene expression defines poor-prognosis subtypes in colorectal cancer. *Nat Genet* 47: 320–329
- Colak S, Ten Dijke P (2017) Targeting TGF-β signaling in cancer. *Trends Cancer* 3: 56–71
- Dominissini D, Moshitch-Moshkovitz S, Schwartz S, Salmon-Divon M, Ungar L, Osenberg S, Cesarkas K, Jacob-Hirsch J, Amariglio N, Kupiec M et al (2012) Topology of the human and mouse m<sup>6</sup>A RNA methylomes revealed by m<sup>6</sup>A-seq. *Nature* 485: 201–206
- Ganesh K, Massague J (2018) TGF-β inhibition and immunotherapy: checkpoint. *Immunity* 48: 626–628
- Guinney J, Dienstmann R, Wang X, De Reynies A, Schlicker A, Sonesson C, Marisa L, Roepman P, Nyamundanda G, Angelino P (2015) The consensus molecular subtypes of colorectal cancer. *Nat Med* 21: 1350–1356
- Han D, Liu J, Chen C, Dong L, Liu Y, Chang R, Huang X, Liu Y, Wang J, Dougherty U (2019) Anti-tumour immunity controlled through mRNA m<sup>6</sup>A methylation and YTHDF1 in dendritic cells. *Nature* 566: 270–274
- Hess ME, Hess S, Meyer KD, Verhagen LA, Koch L, Bronnke HS, Dietrich MO, Jordan SD, Saletore Y, Elemento O et al (2013) The fat mass and obesity associated gene (Fto) regulates activity of the dopaminergic midbrain circuitry. *Nat Neurosci* 16: 1042–1048
- Huff S, Tiwari SK, Gonzalez GM, Wang Y, Rana TM (2021) M(6)A-RNA demethylase FTO inhibitors impair self-renewal in glioblastoma stem cells. *ACS Chem Biol* 16: 324–333
- Huff S, Kummetha IR, Zhang L, Wang L, Bray W, Yin J, Kelley V, Wang Y, Rana TM (2022) Rational design and optimization of m(6)A-RNA demethylase FTO inhibitors as anticancer agents. *J Med Chem* 65: 10920–10937
- Ikushima H, Miyazono K (2010) TGFβ signaling: a complex web in cancer progression. *Nat Rev Cancer* 10: 415–424
- Itatani Y, Kawada K, Sakai Y (2019) Transforming growth factor-β signaling pathway in colorectal cancer and its tumor microenvironment. *Int J Mol Sci* 20: 5822
- Jayaraman M, Ansell SM, Mui BL, Tam YK, Chen J, Du X, Butler D, Eltepu L, Matsuda S, Narayanannair JK (2012) Maximizing the potency of siRNA lipid nanoparticles for hepatic gene silencing *in vivo*. *Angew Chem Int Ed* 124: 8657–8661
- Jung B, Staudacher JJ, Beauchamp D (2017) Transforming growth factor beta superfamily signaling in development of colorectal cancer. *Gastroenterology* 152: 36–52
- Keith JM, Ensinger MJ, Moss B (1978) HeLa cell RNA (2'-O-methyladenosine-N<sup>6</sup>-methyltransferase specific for the capped 5'-end of messenger RNA. *J Biol Chem* 253: 5033–5039
- Kim K, Skora AD, Li Z, Liu Q, Tam AJ, Blosser RL, Diaz LA, Papadopoulos N, Kinzler KW, Vogelstein B (2014) Eradication of metastatic mouse cancers resistant to immune checkpoint blockade by suppression of myeloid-derived cells. *Proc Natl Acad Sci USA* 111: 11774–11779
- Li A, Chen YS, Ping XL, Yang X, Xiao W, Yang Y, Sun HY, Zhu Q, Baidya P, Wang X et al (2017) Cytoplasmic m<sup>6</sup>A reader YTHDF3 promotes mRNA translation. *Cell Res* 27: 444–447
- Li N, Kang Y, Wang L, Huff S, Tang R, Hui H, Agrawal K, Gonzalez GM, Wang Y, Patel SP et al (2020) ALKBH5 regulates anti-PD-1 therapy response by modulating lactate and suppressive immune cell accumulation in tumor microenvironment. *Proc Natl Acad Sci USA* 117: 20159–20170
- Liu J, Yue Y, Han D, Wang X, Fu Y, Zhang L, Jia G, Yu M, Lu Z, Deng X et al (2014) A METTL3-METTL14 complex mediates mammalian nuclear RNA N<sup>6</sup>-adenosine methylation. *Nat Chem Biol* 10: 93–95
- Meyer KD, Saletore Y, Zumbo P, Elemento O, Mason CE, Jaffrey SR (2012) Comprehensive analysis of mRNA methylation reveals enrichment in 3' UTRs and near stop codons. *Cell* 149: 1635–1646
- Mu Y, Yan X, Li D, Zhao D, Wang L, Wang X, Gao D, Yang J, Zhang H, Li Y (2018) NUPR1 maintains autolysosomal efflux by activating SNAP25 transcription in cancer cells. *Autophagy* 14: 654–670
- Muhammad N, Bhattacharya S, Steele R, Phillips N, Ray RB (2017) Involvement of c-Fos in the promotion of cancer stem-like cell properties in head and neck squamous cell carcinoma. *Clin Cancer Res* 23: 3120–3128
- Otegbeye F, Ojo E, Moreton S, Mackowski N, Lee DA, de Lima M, Wald DN (2018) Inhibiting TGF-β signaling preserves the function of highly activated, *in vitro* expanded natural killer cells in AML and colon cancer models. *PLoS One* 13: e0191358
- Pandey MK, Liu G, Cooper TK, Mulder KM (2012) Knockdown of c-Fos suppresses the growth of human colon carcinoma cells in athymic mice. *Int J Cancer* 130: 213–222

- Pandey RR, Delfino E, Homolka D, Roithova A, Chen K-M, Li L, Franco G, Vågbo CB, Taillebourg E, Fauvarque M-O (2020) The mammalian cap-specific m6Am RNA methyltransferase PCIF1 regulates transcript levels in mouse tissues. *Cell Rep* 32: 108038
- Paris J, Morgan M, Campos J, Spencer GJ, Shmakova A, Ivanova I, Mapperley C, Lawson H, Wotherspoon DA, Sepulveda C *et al* (2019) Targeting the RNA m(6)a reader YTHDF2 selectively compromises cancer stem cells in acute myeloid leukemia. *Cell Stem Cell* 25: 137–148.e6
- Paul S, Lal G (2017) The molecular mechanism of natural killer cells function and its importance in cancer immunotherapy. *Front Immunol* 8: 1124
- Saez E, Rutberg SE, Mueller E, Oppenheim H, Smoluk J, Yuspa SH, Spiegelman BM (1995) c-Fos is required for malignant progression of skin tumors. *Cell* 82: 721–732
- Satterlee JS, Basanta-Sanchez M, Blanco S, Li JB, Meyer K, Pollock J, Sadri-Vakili G, Rybak-Wolf A (2014) Novel RNA modifications in the nervous system: form and function. *J Neurosci* 34: 15170–15177
- Schwartz S, Mumbach MR, Jovanovic M, Wang T, Maciag K, Bushkin GG, Mertins P, Ter-Ovanesyan D, Habib N, Cacchiarelli D *et al* (2014) Perturbation of m6A writers reveals two distinct classes of mRNA methylation at internal and 5' sites. *Cell Rep* 8: 284–296
- Sendinc E, Valle-Garcia D, Dhall A, Chen H, Henriques T, Navarrete-Perea J, Sheng W, Gygi SP, Adelman K, Shi Y (2019) PCIF1 catalyzes m6Am mRNA methylation to regulate gene expression. *Mol Cell* 75: 620–630.e9
- Sharma P, Hu-Lieskovan S, Wargo JA, Ribas A (2017) Primary, adaptive, and acquired resistance to cancer immunotherapy. *Cell* 168: 707–723
- Su R, Dong L, Li C, Nachtergaele S, Wunderlich M, Qing Y, Deng X, Wang Y, Weng X, Hu C *et al* (2018) R-2HG exhibits anti-tumor activity by targeting FTO/m(6)a/MYC/CEBPA signaling. *Cell* 172: 90–105.e23
- Sun H, Zhang M, Li K, Bai D, Yi C (2019) Cap-specific, terminal N6-methylation by a mammalian m6Am methyltransferase. *Cell Res* 29: 80–82
- Sung H, Ferlay J, Siegel RL, Laversanne M, Soerjomataram I, Jemal A, Bray F (2021) Global cancer statistics 2020: GLOBOCAN estimates of incidence and mortality worldwide for 36 cancers in 185 countries. *CA Cancer J Clin* 71: 209–249
- Tartell MA, Boulias K, Hoffmann GB, Bloyet LM, Greer EL, Whelan SPJ (2021) Methylation of viral mRNA cap structures by PCIF1 attenuates the antiviral activity of interferon-beta. *Proc Natl Acad Sci USA* 118: e2025769118
- Vu LP, Pickering BF, Cheng Y, Zaccara S, Nguyen D, Minuesa G, Chou T, Chow A, Saletore Y, MacKay M (2017) The N6-methyladenosine (m6A)-forming enzyme METTL3 controls myeloid differentiation of normal hematopoietic and leukemia cells. *Nat Med* 23: 1369–1376
- Wang X, Lu Z, Gomez A, Hon GC, Yue Y, Han D, Fu Y, Parisien M, Dai Q, Jia G (2014) N6-methyladenosine-dependent regulation of messenger RNA stability. *Nature* 505: 117–120
- Wang X, Zhao BS, Roundtree IA, Lu Z, Han D, Ma H, Weng X, Chen K, Shi H, He C (2015) N6-methyladenosine modulates messenger RNA translation efficiency. *Cell* 161: 1388–1399
- Wang L, Hui H, Agrawal K, Kang Y, Li N, Tang R, Yuan J, Rana TM (2020) M(6) a RNA methyltransferases METTL3/14 regulate immune responses to anti-PD-1 therapy. *EMBO J* 39: e104514
- Wang L, Sun J, Yin Y, Sun Y, Ma J, Zhou R, Chang X, Li D, Yao Z, Tian SJ *et al* (2021) Transcriptional coregulator NUPR1 maintains tamoxifen resistance in breast cancer cells. *Cell Death Dis* 12: 1–16
- Wei C, Gershowitz A, Moss B (1975) N6, O2'-dimethyladenosine a novel methylated ribonucleoside next to the 5' terminal of animal cell and virus mRNAs. *Nature* 257: 251–253
- Wei L-H, Song P, Wang Y, Lu Z, Tang Q, Yu Q, Xiao Y, Zhang X, Duan H-C, Jia G (2018) The m6A reader ECT2 controls trichome morphology by affecting mRNA stability in *Arabidopsis*. *Plant Cell* 30: 968–985
- Xiao W, Adhikari S, Dahal U, Chen Y-S, Hao Y-J, Sun B-F, Sun H-Y, Li A, Ping X-L, Lai W-Y (2016) Nuclear m6A reader YTHDC1 regulates mRNA splicing. *Mol Cell* 61: 507–519
- Xu Y, Pasche B (2007) TGF-β signaling alterations and susceptibility to colorectal cancer. *Hum Mol Genet* 16: R14–R20
- Yang S, Wei J, Cui Y-H, Park G, Shah P, Deng Y, Aplin AE, Lu Z, Hwang S, He C (2019) m6A mRNA demethylase FTO regulates melanoma tumorigenicity and response to anti-PD-1 blockade. *Nat Commun* 10: 2782
- Yankova E, Blackaby W, Albertella M, Rak J, De Braekeleer E, Tsagkogeorga G, Pilka ES, Aspris D, Leggate D, Hendrick AC (2021) Small-molecule inhibition of METTL3 as a strategy against myeloid leukaemia. *Nature* 593: 597–601
- Zhang Q, Kang Y, Wang S, Gonzalez GM, Li W, Hui H, Wang Y, Rana TM (2021) HIV reprograms host m(6)Am RNA methylome by viral Vpr protein-mediated degradation of PCIF1. *Nat Commun* 12: 5543
- Zheng G, Dahl JA, Niu Y, Fedorcsak P, Huang C-M, Li CJ, Vågbo CB, Shi Y, Wang W-L, Song S-H (2013) ALKBH5 is a mammalian RNA demethylase that impacts RNA metabolism and mouse fertility. *Mol Cell* 49: 18–29
- Zhou P, Wan X, Zou Y, Chen Z, Zhong A (2020) Transforming growth factor beta (TGF-β) is activated by the CtBP2-p300-AP1 transcriptional complex in chronic renal failure. *Int J Biol Sci* 16: 204–215



**License:** This is an open access article under the terms of the [Creative Commons Attribution-NonCommercial-NoDerivs](https://creativecommons.org/licenses/by-nc-nd/4.0/) License, which permits use and distribution in any medium, provided the original work is properly cited, the use is non-commercial and no modifications or adaptations are made.